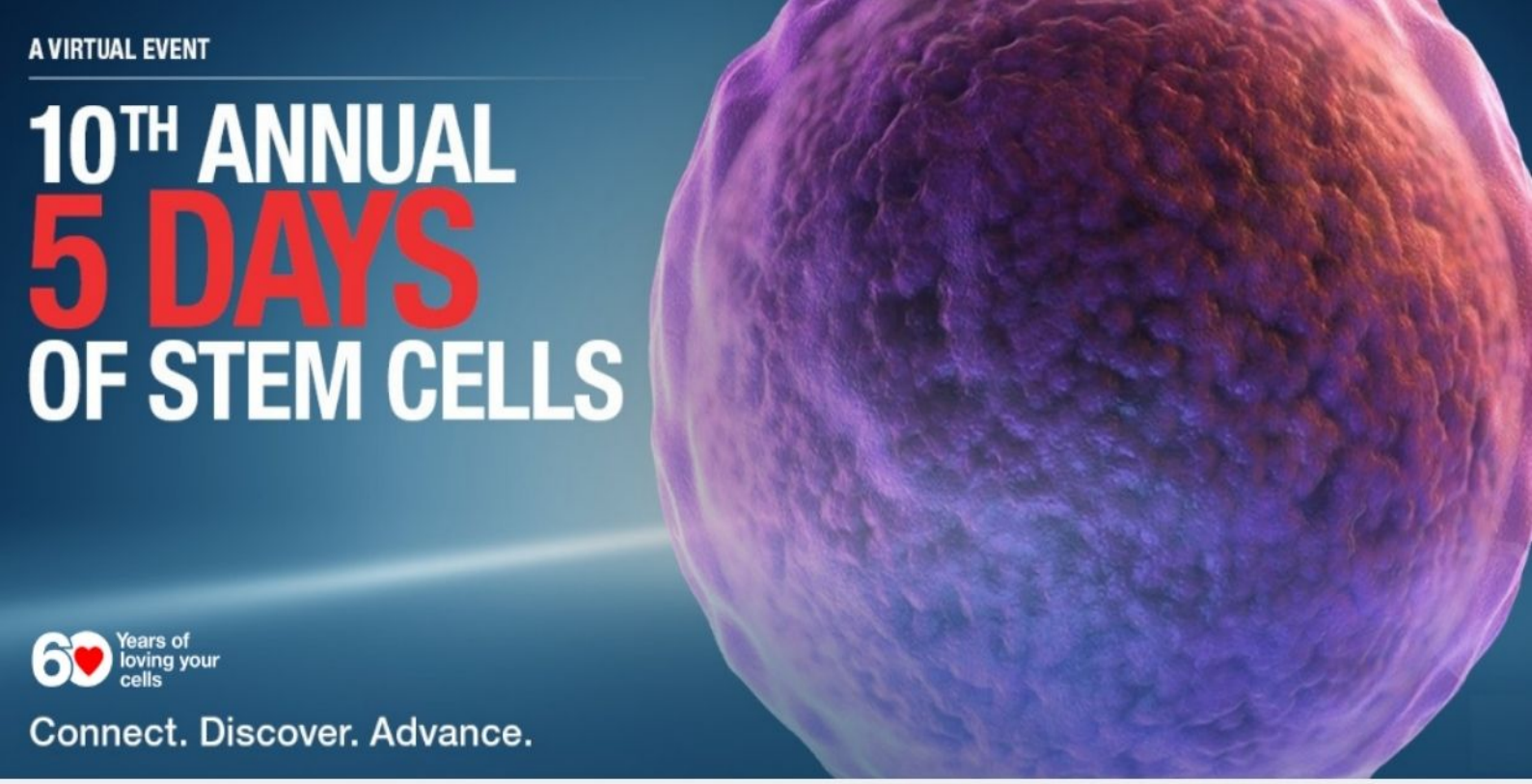


## Join us for the world's leading virtual Stem Cell event

## October 31 – November 4

**The program includes various sessions in:**

- 3D culture/organoid
- Cell therapies
- Stem cell best practices
- Reprogramming & gene editing
- Workflow optimization
- Future of stem cells

**What's in it for you?**

- Gain and share insights and discuss industry trends.
- Celebrate Gibco's 60th anniversary: play and win prizes
- Network with your peers directly
- Receive a certificate of attendance

Thermofisher.com/5daysofstemcells

WILEY CURRENT PROTOCOLS A Wiley Brand gibco ThermoFisher SCIENTIFIC

Bozic Ivan (Orcid ID: 0000-0002-3233-9936)

# Coupling between the prelimbic cortex, nucleus reuniens, and hippocampus during NREM sleep remains stable under cognitive and homeostatic demands

Running title: Nucleus reuniens modulates coupling of cortical slow waves and spindles to hippocampal ripples during NREM sleep

Ivan Bozic[1,2], Thomas Rusterholz[1,2], Christian Mikutta[3,4,5], Carlos del Rio Bermudez[1,2], Christoph Nissen[3] & Antoine Adamantidis[1,2,5]

[1] Zentrum für Experimentelle Neurologie, Department of Neurology, Inselspital University Hospital Bern, Bern, Switzerland.

[2] Department of Biomedical Research, University of Bern, Bern, Switzerland.

[3] University Hospital of Psychiatry and Psychotherapy, University of Bern, Switzerland

[4] Privatklinik Meiringen, Meiringen, Switzerland

[5] Department of Physiology, Anatomy and Genetics, University of Oxford

**Keywords:** Nucleus reuniens thalami, cortico-hippocampal communication, oscillations, sleep, memory consolidation

[5]To whom correspondence may be addressed. Email: antoine.adamantidis@dbmr.unibe.ch.



This article has been accepted for publication and undergone full peer review but has not been through the copyediting, typesetting, pagination and proofreading process which may lead to differences between this version and the Version of Record. Please cite this article as doi: 10.1111/ejn.15853

**Abstract**

The interplay between the medial prefrontal cortex and hippocampus during non-REM (NREM) sleep contributes to the consolidation of contextual memories. To assess the role of the thalamic nucleus reuniens (Nre) in this interaction, we investigated the coupling of neuro-oscillatory activities between prelimbic cortex, Nre, and hippocampus across sleep states and their role in the consolidation of contextual memories using multi-site electrophysiological recordings and optogenetic manipulations. We showed that ripples are time-locked to the Up state of cortical slow waves, the transition from Up to Down state in thalamic slow waves, the troughs of cortical spindles, and the peaks of thalamic spindles during spontaneous sleep, rebound sleep, and sleep following a fear conditioning task. In addition, spiking activity in Nre increased before hippocampal ripples and the phase-locking of hippocampal ripples and thalamic spindles during NREM sleep was stronger after acquisition of a fear memory. We showed that optogenetic inhibition of Nre neurons reduced phase-locking of ripples to cortical slow waves in the ventral hippocampus while their activation altered the preferred phase of ripples to slow waves in ventral and dorsal hippocampi. However, none of these optogenetic manipulations of Nre during sleep after acquisition of fear conditioning did alter sleep-dependent memory consolidation. Collectively, these results showed that Nre is central in modulating hippocampus and cortical rhythms during NREM sleep.

**Introduction**

Non-rapid eye movement (NREM) sleep is characterized by behavioral quiescence and heightened response threshold to sensory or environmental stimuli. During this state, key electroencephalographic (EEG) features in humans and rodents include a shift towards high-amplitude, low-frequency oscillatory activities (<4Hz) and the occurrence of discrete phenomena such as slow waves (Steriade, 2000), sleep spindles (McCormick & Bal, 1997) and sharp-wave ripples (Buzsáki, 2015). While sleep spindles and slow waves occur within thalamo-cortical networks (Crunelli et al., 2018; McCormick & Bal, 1997; Steriade et al., 1993), sharp-wave ripples are generated within the hippocampal formation (Adamantidis et al., 2019; Buzsáki, 2015). Crucially, cortical slow waves and spindles have been shown to co-occur with ripples in the hippocampus (HPC) (Clemens et al., 2007, 2011; Jiang et al., 2019; Siapas & Wilson, 1998; Sirota et al., 2003). Indeed, some of the ripples are temporally locked to the troughs of spindles (Phillips et al., 2012; Sirota et al., 2003; Staresina et al., 2015) and the UP state of slow waves (Mölle et al., 2009; Sirota et al., 2003) in the medial prefrontal cortex (mPFC) in rodents. Studies in humans revealed that coupling between ripples and slow waves or spindles also occurred between the HPC and many other cortical areas including parietal and occipital regions, with a preference for frontal regions (Clemens et al., 2007, 2011; Jiang et al., 2019).

Neural oscillatory activity is thought to support brain plasticity (Diekelmann & Born, 2010; Puentes-Mestril & Aton, 2017; Tononi & Cirelli, 2014) and memory consolidation. In particular, the coupling of hippocampal ripples to slow waves and spindles in the prefrontal cortex (PFC) during NREM sleep is thought to be implicated in the consolidation of fear memories through replay processes during sleep (Klinzing et al., 2019; Marr et al., 1991). Indeed, the temporal locking of hippocampal ripples to UP states of prefrontal slow waves in

rats has been shown to increase after a learning task (Maingret et al., 2016; Mölle et al., 2009). Furthermore, mice that were sleep deprived immediately following a hippocampus-dependent conditioning task did not show an increase in sharp wave ripple activity during recovery sleep compared to mice that were allowed to sleep immediately after the conditioning task (Li et al., 2021), supporting the idea that neural oscillatory activity facilitates memory consolidation. Along this line, while the suppression of hippocampal ripples during NREM sleep impaired performance in a radial-maze task in rats (Girardeau et al., 2009), enhancing coupling of ripples to both cortical slow waves (Maingret et al., 2016) and spindles (Latchoumane et al., 2017) improved contextual memory performance.

Both anatomically and functionally, different aspects of memories are encoded by different parts of the HPC and PFC. The prelimbic part of the PFC is implicated in the expression of fear memory (Sierra-Mercado et al., 2011; Sotres-Bayon et al., 2012) and the encoding of danger- versus safety-associated cues (Aime et al., 2020; Likhtik & Paz, 2015; Vidal-Gonzalez et al., 2006). The dorsal HPC is implicated in spatial aspects during environmental exploration or goal directed tasks, while the ventral portion of HPC is implicated in emotional and social aspects (Fanselow & Dong, 2010; Jimenez et al., 2020). On an anatomical basis, while neurons in the ventral parts of the HPC and subiculum project directly to the PFC (Gabbott et al., 2002), neurons in the dorsal HPC are indirectly connected to the PFC via relays located in the basal ganglia and thalamus (Thierry et al., 2000).

Connections from the PFC to HPC are primarily relayed through the peri- and enthorhinal cortices (Apergis-Schoute et al., 2006) and the midthalamic *nucleus reuniens* (Nre) (Cassel et al., 2013; Varela et al., 2014). Anatomically, the Nre is uniquely located to play a role in the coordination of cortico-hippocampal activity as it is reciprocally connected to mPFC (including prelimbic and infralimbic cortices) and the hippocampal formation through axonal projections to the CA1 stratum lacunosum moleculare and additional inputs from the subiculum (Cassel et al., 2013; Dolleman-van der Weel et al., 2019; Varela et al., 2014). In addition, the Nre is reciprocally connected to the amygdala, which plays a key role in the expression of fear behavior (Duvarci & Pare, 2014).

Because of the aforementioned anatomical features, Nre neurons support associative behaviors through their influence on HPC and PFC networks, including the acquisition, consolidation, and recall of fear memories (Jin & Maren, 2015). Indeed, inactivating Nre neurons using local injections of the GABA agonist muscimol prior to a fear extinction procedure impaired the acquisition of both short- and long-term extinction memories in rats (Ramanathan & Maren, 2019). Muscimol inactivation of Nre neurons prior to fear conditioning in rats also impaired the acquisition of a fear memory in contextual fear conditioning while its administration before recall led to generalized freezing to a novel context with no effects on auditory discrimination during a fear conditioning task (Ramanathan et al., 2018). In addition, local muscimol injection in Nre of rats impaired retrieval of spatial memory in a crossword-like maze looking for a reward (Mei et al., 2018). In contrast, the role of Nre in memory consolidation remains unclear. Inhibition of Nre neurons either has no effect (Mei et al., 2018) or leads to generalization of contextual memory after fear conditioning in mice

(Troyner et al., 2018; Xu & Sudhof, 2013). Finally, several studies demonstrated Nre's implication in consolidation of remote memories (i.e., after at least 21 days) (Ali et al., 2017; Loureiro et al., 2012; Quet et al., 2020; Troyner et al., 2018).

At circuit level, studies have shown that Nre neurons modulated the coherence of delta frequency oscillations (Hauer et al., 2019; Roy et al., 2017), the synchrony of gamma-bursts (Ferraris et al., 2018) between PFC and HPC in urethane anesthetized rats, as well as firing sequences of neurons in the HPC and PFC during slow waves (Angulo-Garcia et al., 2020). In addition, Nre neurons mediate theta coherence, theta-gamma coupling and directionality between cortex and HPC during a spatial working memory task and support performance in the task (Hallock et al., 2016). Altogether these studies suggested the involvement of Nre neurons in behaviors implicating cortico-hippocampal communication during both wakefulness and sleep.

Thus, in this study we assessed the involvement of Nre neurons in the temporal coordination of cortical slow waves and spindles with hippocampal ripples during NREM sleep, and associated memory consolidation in mice using electrophysiological recordings and optogenetics.

**Results**

First, we quantified the densities and coordination of sleep oscillations, i.e., synchrony of slow waves, spindles, and ripples in mPFC, Nre and CA1 after sleep deprivation or a learning task. Changes in spindle density during sleep after learning and sleep deprivation have been demonstrated for cortical regions (Eschenko et al., 2006; Gais et al., 2002; Knoblauch et al., 2003) but not for Nre. Higher ripple densities during sleep were described after learning (Eschenko et al., 2008) but not after sleep deprivation. As mentioned above, ripples co-occur with cortical spindles and slow waves with a preference of ripples to be nested in the UP state of slow waves (Mölle et al., 2009; Sirota et al., 2003) and the troughs of spindles (Phillips et al., 2012; Sirota et al., 2003; Staresina et al., 2015) while coupling of these oscillations increased after learning (Maingret et al., 2016; Mölle et al., 2009). However, the densities and stability of phase-locking of hippocampal ripples to UP states and spindle troughs remains stable after sleep deprivation and learning remain sparsely described (Mölle et al., 2009). To test this, we simultaneously recorded neural activities between mPFC, HPC and Nre across different sleep-wake states and experimental conditions. We stereotactically implanted male mice with multi-site electrodes in Nre, ventral and dorsal portion of CA1 (vCA1 and dCA1), and the prelimbic portion of the mPFC (Prl) on the left hemisphere. To assess sleep-wake states, EEG and electromyographic electrodes (EMG) were chronically implanted (Fig.1a-b, supp. fig. 1a). After recovery, mice underwent three experimental sleep conditions, namely unperturbed sleep ('baseline', BL), sleep after deprivation ('rebound sleep', Reb), and sleep after memory acquisition in an auditory contextual fear conditioning paradigm ('post-learning sleep', PL, see methods for details). These conditions aimed at testing possible effects of heightened homeostatic and mnemonic demands on the dynamics of the PFC-Nre-HPC network (Fig.1c-d, supp.fig.1b-c, supp. table 1). Local field potential (LFP), EEG and EMG signals were recorded during natural sleep for 5 hours following experimental procedures (Fig.1e).

**Slow waves and spindles in prelimbic cortex and Nre are coupled to and drive hippocampal ripples**

One aim of the study was to characterise the temporal coupling between spindles and slow waves in thalamo-cortical networks (Fig.1f, g), and sharp-wave ripples in the vCA1 and dCA1 (Fig.1h). In a first step, we quantified the occurrence of spindles and ripples over the course of NREM sleep (i.e., densities) as an indication of potential changes in cross-frequency coupling (see methods for concatenation of NREM sleep episodes; Fig.1i). During the first half hour of 'rebound sleep' both spindles in Nre ($F_{condition}$= 1.5, $F_{time}$= 9.2, $F_{time\ x\ condition}$= 3.6; Fig.1i, bottom left) and Prl ($F_{condition}$= 0.4, $F_{time}$= 9.2, $F_{time\ x\ condition}$= 4.1; Fig.1i, bottom right), and ripple events in vCA1 ($F_{condition}$= 0.5, $F_{time}$= 16.1, $F_{time\ x\ condition}$= 3.7; Fig.1i, top right) showed higher occurrence densities than during baseline which were not present in spindles measured from frontal EEG (supp. fig. 1d), suggesting a potential homeostatic response for these events. As compared with baseline, post-learning sleep showed higher ripple densities in dCA1 for the entire first hour of NREM sleep ($F_{condition}$= 2.3, $F_{time}$= 35.1, $F_{time\ x\ condition}$= 5.7; Fig.1i, top left). This result suggested the involvement of hippocampal ripples in sleep-dependent memory consolidation consistent with previous findings describing higher ripple densities after learning (Eschenko et al., 2008), suggesting the involvement of hippocampal ripples in sleep-dependent memory consolidation (Maingret et al., 2016; Mölle et al., 2009). Since the event densities were significantly elevated for the first half hour of rebound sleep and for the first hour of post-learning sleep, these time windows were selected for the subsequent LFP and spike analyses of this experiment and compared to total sleep time during baseline sleep.

Thus, we first calculated the total event density during total baseline sleep, the first 30min of rebound sleep and the first hour of post-learning sleep. We found a significant increase of thalamo-cortical slow waves and cortical spindles after both rebound sleep and post-learning compared to baseline conditions (Prl slow waves: F= 11.1, P for Reb= 0.0002, P for PL= 0.0139. Nre slow waves: F=5.7, P for Reb= 0.009, P for PL= 0.0274. Prl spindles: F=24.7, P for Reb <0.0001, P for PL= 0.0385) as well as an increase in dCA1 ripples in post-learning sleep (F= 2.97, P= 0.0494; Fig.2a, supp. table 2). Next, we investigated the amount of hippocampal ripples that occur at the time of thalamo-cortical slow waves and spindles (see methods). We found that the amount of ripples coupled to slow waves during rebound sleep and post-learning sleep was also increased as compared to baseline conditions (Nre-vCA1: F= 16.8, P for Reb= 0.0017, P for PL<0.0001; Nre-dCA1: F= 14.97, P for Reb<0.0001, P for PL= 0.0018; Pfl-vCA1: F=17.1, P for Reb<0.0001, P for PL= 0.003; Prl-dCA1: F=6.684, P for Reb= 0.0042; Fig.2b top, supp. table 3). The coupling of hippocampal ripples to spindles remained stable across conditions (Fig.2b bottom, supp. table 3). To rule out whether the increased co-occurrence rates of slow waves and ripples in all electrode pairs in rebound and post-learning sleep resulted from the increase of oscillatory events, we calculated the rate of co-occurrence using data, where we shuffled the time stamps of ripples, slow waves, and spindles 100 times and calculated the ratio of observed and shuffled occurrence rates. We found that coupling of ripples to slow waves in both Nre and Prl occurred at rates that were between chance level and 1.4 times above chance level (Fig.2c top, supp. table 3). Coupling of thalamic spindles to ripples occurred at a rate that was 2-3 times higher than chance level.

(Fig.2c bottom, supp. table 3).

However, the aforementioned increases in the co-occurrence rate of slow waves and ripples observed during rebound sleep and post-learning sleep as compared to baseline sleep were not present anymore, suggesting that they resulted from the higher densities of slow waves, spindles, and ripples.

Next, we tested whether hippocampal ripples occur at specific phases of slow wave and spindle oscillatory activity in Prl and Nre, as shown for cortical recordings in humans and rats (Jiang et al., 2019; Mölle et al., 2009; Staresina et al., 2015). Specifically, we performed phase-amplitude coupling analyses for ripples that co-occur with a slow wave or a spindle by first extracting the phase of Prl and Nre traces that were filtered in slow wave range (0.5-4Hz) or spindle range (9-16Hz), respectively. Next, we extracted the phase of the slow wave or spindle at which each ripple occured and calculated the mean circular vector of all extracted phase values to quantify the coupling of ripples to the phase of thalamic and cortical slow waves and spindles (see methods). We found that ripples in both ventral and dorsal CA1 were preferentially locked to the UP state (shortly after 0°, positive slope) of slow waves in the cortex. As for the coupling to thalamic slow waves, ripples from both parts of CA1 occurred at the transition from UP to DOWN state (around 90°). Similarly, to previous studies (Phillips et al., 2012; Staresina et al., 2015), ripples fell into the trough of spindles in Prl and onto the peak of spindles in Nre. We observed a significant increase in the phase-locking of vCA1 ripples to Nre spindles in post-learning sleep and a shift in the preferred phase in rebound sleep ($F=14.5$, $P<0.0001$ in Reb, $P= 0.0192$ in PL). These were accompanied by a shift in the preferred phase of vCA1 ripples to Nre slow waves in post-learning sleep and a reduced phase-locking during rebound sleep ($F=110.1$, $P <0.0001$ in both Reb and PL). To a lesser extent, we also found a shift in the preferred phase of dCA1 ripples to Nre slow waves in post-learning sleep ($F=77$, $P<0.0001$), a shift in the preferred phase of vCA1 ripples to Prl slow waves in post-learning sleep and a reduced phase-locking during rebound sleep ($F=44.9$, $P=0.0109$ in Reb, $P<0.0001$ in PL). These changes were associated with a reduced phase-locking and shift in the preferred phase of dCA1 ripples to Prl slow waves in post-learning sleep ($F=31.7$, $P<0.0001$), shifts in the preferred phase of dCA1 ripples to Nre spindles in rebound and post-learning sleep as well as an increased phase-locking in post-learning sleep ($F=19.8$, $P= 0.0002$ in Reb, $P<0.0001$ in PL), and an increased phase-locking of vCA1 ripples to Prl spindles in post-learning sleep ($F=4.8$, $P=0.0316$, Fig.2d, supp. table 3). These findings suggested that subtle changes in oscillations synchrony are associated with increased homeostatic or mnemonic needs.

To assess the directionality (i.e., flow of information) of these oscillatory events, we next calculated the phase slope index (PSI), see methods for further details. We found that both slow waves and spindles in cortex and thalamus drove hippocampal ripples (negative values indicate that ripples drove slow waves/spindles; Fig.2e, supp. table 3). Interestingly, even though the phase-locking of ripples to slow waves during rebound sleep did not change, we observed significant increases in the directional strength of slow waves and spindles onto

ripples. This was marked by a significant increase of the drive of Nre slow waves onto vCA1 and dCA1 ripples during rebound sleep. To a lesser extent, Prl slow waves showed an increase of the drive on vCA1 ripples as well (Nre-vCA1: F= 12.5, P=0.0001; Nre-dCA1: F= 14.2, P <0.0001, Prl-vCA1: F= 6.2, P = 0.0043). Additionally, Prl spindles showed a robustly increased drive onto all ripples during rebound sleep, while this was also observed for Nre spindles onto dCA1 ripples as well. Intriguingly, both thalamic and cortical spindles showed an increased drive onto all ripples during post-learning sleep (Nre-vCA1: F= 3.2, P for PL= 0.0376; Nre-dCA1: F= 4.03, P for Reb= 0.0471, P for PL= 0.042; Prl-vCA1: F= 3.4 P for Reb <0.0001, P for PL= 0.0088; Prl-dCA1: F= 2.4, P for Reb= 0.0003, P for PL= 0.0057). These results suggested an influence of homeostatic and mnemonic needs on the directionality between slow waves or spindles and ripples.

Collectively, these results confirmed the coupling of cortical slow waves. Furthermore, both thalamic and cortical slow waves and spindles exert a drive on hippocampal ripples, consistent with a previous study (Helfrich et al., 2019).

**Nucleus reuniens single-unit activity is locked to hippocampal ripples**

To investigate the firing characteristics of Nre neurons across behavioral states in baseline, rebound sleep and post-learning sleep, single units from Nre neurons were sorted from multi-unit recordings (MUA) and their spike rate in all three conditions was calculated (see Methods; Fig.3a). We found that during baseline sleep, Nre cells fired at 14.2 ±2.6Hz during wake, 5.6 ±0.8Hz during NREM sleep and 7.6 ±0.8Hz during REM sleep (Fig.3b). During rebound sleep, Nre cells showed spike rates of 11.5 ±3.7Hz during wake, 7.2 ±1.8Hz during NREM sleep and 6.5 ±1.3Hz during REM sleep. During post-learning sleep, spike rates were 19.02 ±2.4Hz during wakefulness, 6.8 ±1.03Hz during NREM sleep and 10.4 ±1.5Hz during REM sleep (baseline sleep: n=11 cells from 8 animals, rebound sleep: n= 11 cells from 6 animals, post-learning sleep: n= 10 cells from 6 animals; Fig 3b). Note that differences in spike rates across experimental conditions were not significant.

Next, we assessed the bursting activity of Nre neurons by calculating their inter spike intervals (Fig3c top). We found that in all conditions Nre neurons displayed bursting activity patterns. Indeed, Nre neurons exhibited 3.6 ±1.6 bursts per minute during baseline sleep, 2.5 ±1.1 bursts/min during rebound sleep and 8.8 ±2.8 bursts/min during post-learning sleep (Fig.3c inset). The occurrence of bursts did not show a clear rhythmicity or significant differences between the experimental conditions (Fig.3c bottom).

To assess the influence of Nre spiking on Prl, which in turn could affect the connectivity between cortex and HPC, we calculated Nre spike rates time-locked to the beginning of UP states in Prl (Fig.3d top). We found a significant increase of Nre spike rates occurring immediately before the beginning of the UP state (lag during baseline sleep: -2.4 ±7.5ms, rebound sleep: -31.1 ±6.99ms, post-learning sleep: -11.1 ±3.8ms; Fig.3d bottom left). The timing and steepness of the increase did not change across conditions (slope during baseline: 12.3 ±6.5 (a.u.), rebound sleep: 7 ±6.1, and post-learning sleep: 6.6 ±3.3; Fig.3d bottom right).

Next, we investigated the spiking behavior of Nre in relation to hippocampal ripples by calculating spike rates time-locked to ripples (Fig.3e) and found a significant increase preceding ripples during baseline sleep (vCA1 P= 0.0078; dCA1 P= 0.0078 using paired sign rank test) and post-learning sleep (vCA1 P= 0.0098; dCA1 P= 0.002), consistent with the observation that ripples occurred at the end of thalamic UP states (Fig.2d). During rebound sleep, the increase of Nre neuron spiking shifted closer towards a later time point and thus occurred together with ripples in dCA1 (P= 0.0078). At the same time, Nre spikes did not show an increase of spike rate locked to ripples in vCA1 but rather a decrease immediately after the ripple (P= 0.0391), likely corresponding to the end of the UP state (Fig.2d). Lastly, we explored Nre spike rates during ripples that were either locked to the UP state of cortical slow waves or troughs of cortical spindles; this analysis did not show any clear patterns (supp. fig.2). The results showed that sleep deprivation potentially leads to a change of Nre spiking behavior in relation to hippocampal ripples through an increase of the spike activity increase during dCA1 ripples and a decrease of spike activity during vCA1 ripples.

**Optogenetic manipulation of nucleus reuniens alters cross-frequency coupling between hippocampus and prelimbic cortex**

To test whether Nre plays a causal role in the functional connectivity between prelimbic cortex and HPC, we used optogenetics to perturb the firing of Nre neurons. To genetically express opsins in Nre neurons, AAV2-CamKII-ChR2-EYFP, AAV2-CamKII-ArchT3.0-EYFP or AAV2-CamKII -EYFP were stereotactically injected in the Nre of male wildtype mice for optogenetic manipulation of Nre neurons in freely moving mice (n=6 per group, see methods, Fig.4a). After 20 days, mice were implanted with chronic multi-site tetrodes in Prl, Nre (except for mice injected with AAV2-CamKII -EYFP), dCA1 and vCA1, EEG and EMG electrodes, and an optic fiber placed above the Nre as previously described (see methods)(Gent et al., 2018). After recovery and habituation to the recording conditions, mice underwent an auditory contextual fear conditioning task to test for a possible Nre involvement in both hippocampus-dependent and independent memory consolidation (see methods, Fig.4b). After acquisition, separate groups of ChR2 and ArchT mice underwent either a NREM sleep-specific optogenetic stimulation or silencing protocol over the first 4h of NREM sleep following conditioning (ChR2: 140 trains of 5-ms pulses delivered at 7Hz; ArchT: continuous 20-second-long pulse; Fig.4c). As shown in the raster plot, our methods were proven effective of silencing (ArchT) and stimulating (ChR2) neurons in Nre. Control mice (EYFP control mice) were evenly assigned to either the stimulating protocol or the silencing protocol. Only LFP data in NREM during stimulation/silencing were considered for the subsequent analyses.

First, a coherence analysis was performed across the relatively short trials with optogenetic stimulation/inhibition permitted it. Note that this was not possible during the hour-long recordings from the previous experiments. We found that optogenetic silencing of ArchT-expressing Nre neurons selectively during NREM sleep led to a significant decrease of coherence of low delta frequency oscillations (1-2Hz) between dCA1 and Prl as compared to control conditions (Fig.4d top). Stimulating tonically at 7Hz led to a decrease in higher frequencies from 6Hz onwards (Fig.4d top). Interestingly, coherence between vCA1 and Prl was

not affected neither by stimulation nor silencing of Nre (Fig.4d bottom).
Based on previous results (Fig.2), we next characterized the phase-amplitude coupling of hippocampal ripples to cortical slow waves and spindles upon optogenetic activating or silencing of Nre neurons during sleep. Both activating and silencing Nre neurons altered the preferred phase of ripples locked to cortical spindles (vCA1 in ArchT P= 0.0074; vCA1 in ChR2 P= 0.0015, F= 8.1; dCA1 ArchT and ChR2 P<0.0001, F= 66.8), while the effects on slow waves were more diverse. Optogenetic activation of ChR2-expressing Nre cells shifted the preferred phase of ripple activity in both vCA1 (F=146.4) and dCA1 (F=100.5) (vCA1 and dCA1 P<0.0001). Optogenetic silencing of ArchT-expressing Nre cells had no effect on ripples in dCA1 while the phase-locking of ripples in vCA1 was significantly reduced (P= 0.0234; Fig.4e, supp. table 4). Next, we found that co-occurrence of ripples with spindles or slow waves, respectively, was also influenced by Nre neuronal firing. Optogenetic activation of ChR2-expressing Nre neurons increased co-occurrence of vCA1 ripples with spindles (F= 3.7, P= 0.0459), while optogentic silencing of ArchT-expressing Nre neurons increased the co-occurrence of dCA1 ripples with slow waves as compared to controls (F= 7.2, P= 0.0037; Fig.4f, supp. table 4). Both findings could not be attributed to higher densities of slow waves, spindles, or ripples, hence the calculation of the ratio of observed/shuffled co-occurrence was irrelevant (supp. fig. 3e-h). Altogether, these results suggested that Nre neurons were not only involved in the precise phase-amplitude coupling between cortical slow waves and spindles and hippocampal ripples, but they also contributed to the initiation of cortical slow waves and spindles in Prl.

Lastly, we calculated the PSI to assess Nre's influence on the directionality of Prl slow waves and spindles, and hippocampal ripples. Both activation and silencing significantly decreased the drive of slow waves on vCA1 ripples compared to the control condition (F= 5.4, P for ChR2= 0.0032, P for ArchT= 0.0061). Additionally, optogenetic silencing of Nre neurons reduced the drive of slow waves onto dCA1 ripples (F=1.7, P= 0.0268; Fig.4g, supp. table 4). We next tested whether optogenetic activation, or silencing, Nre neurons during post-learning NREM sleep had an effect on memory consolidation of both hippocampus-dependent and hippocampus-independent fear memory. Despite the significant changes in cortico-hippocampal cross-frequency coupling upon optogenetic perturbation, there were no significant changes in neither contextual memory performance nor hippocampus-independent cue learning (Fig.4h, see also supp. table 5).

## Discussion

The Nre has been implicated in a variety of functions that involve prefrontal-hippocampal communication, such as acquisition, retention, and recall of contextual memories (Davoodi et al., 2011; Lin et al., 2020; Mei et al., 2018; Ornelas et al., 2021; Ramanathan et al., 2018; Ramanathan & Maren, 2019; Schwabe et al., 2021), as well as spatial working memory (Hallock et al., 2013, 2016; Layfield et al., 2015; Maisson et al., 2018). Additionally, the Nre is thought to play a role in re- and destabilization of fear-related memories as well as in their specificity (Troyner & Bertoglio, 2020, 2021; Xu & Sudhof, 2013). However, its involvement

in consolidation of hippocampus-dependent memories is less clear. One study found no effect in a maze task after inhibiting Nre during the consolidation phase (Mei et al., 2018), while another reported a more generalized expression of fear and stronger persistence of fear memory after contextual fear conditioning and Nre inhibition with muscimol during the consolidation phase (Troyner et al., 2018). A third study found weaker performance in a passive avoidance task when Nre was inhibited using tetracaine immediately after acquisition (Davoodi et al., 2011).

In the present study, we showed that neural oscillations in the Nre and prelimbic cortex are time-locked to sharp-wave ripples in the hippocampus and that this coupling remains stable during sleep after sleep deprivation and after acquisition of a fear conditioning task (learning). We showed that only a fraction (20-40%) of hippocampal ripples co-occur with cortical or thalamic slow waves, and with spindles (3-8%). These results extended the quantification of discrete events as compared to Siapas and Wilson in 1998 which provided correlation-coefficients of events in rats (Siapas & Wilson, 1998) and ripple activity in relation to slow waves and spindles in humans (Clemens et al., 2011). Even though the observed increases in co-occurrence were mainly due to higher densities of all events, higher co-occurrence of these oscillations may contribute to information transfer from HPC to cortex, as proposed by the *systems memory consolidation* hypothesis (Klinzing et al., 2019). Our findings are complementary to the findings of Maingret et al. that showed an increased co-occurrence after a fear conditioning task relative to a baseline recording, and possibly a similar increase in their respective densities (Maingret et al., 2016). Furthermore, we confirmed that ripples tend to occur during a cortical UP state (Clemens et al., 2007; Mölle et al., 2009; Oyanedel et al., 2020; Sirota et al., 2003; Sirota & Buzsaki, 2005) and during troughs of spindles (Phillips et al., 2012; Sirota et al., 2003; Staresina et al., 2015). We also showed that ripples are coupled to the end of the UP state (reflected in both LFP and potentially also spike analyses) and the peak of spindles in thalamic Nre. The most striking changes were the increased phase-locking of vCA1 ripples to Nre spindles during post-learning sleep, a shift towards the Down state in the locking of vCA1 ripples to Nre slow waves during post-learning sleep and a reduced phase-locking during rebound sleep. However, we did not confirm the increased phase-locking of dCA1 ripples with prefrontal slow waves after a learning task as described before (Mölle et al., 2009). This discrepancy is possibly due to the usage of EEG instead of LFP electrodes and a different type of learning task, i.e. odor-learning task vs. fear conditioning. Additionally, despite low sampling, Nre spiking shows a peak before the occurrence of hippocampal ripples. This constellation of ripples locking to thalamic spindle peaks and Nre neurons showing a peak in their spiking activity right before ripples supports the findings of a previous study which showed that precise timing of Nre spikes and spikes of pyramidal CA1 neurons modulates spike-timing related plasticity in PFC (Banks et al., 2021). Despite the low sampling, we still observed, that the activity of Nre neurons is modulated in relation to hippocampal ripples and cortical slow waves. Yet, these observations remain to be confirmed in future investigations using higher throughput experimental approaches. Both rebound sleep and post-learning sleep displayed elevated densities of spindles, ripples, and slow waves in the first 30min or in the first hour, respectively. The elevation of spindle

densities contrasted with the drop in spindle densities after sleep deprivation observed in humans (Dijk et al., 1993; Knoblauch et al., 2003) and in mice (Vyazovskiy et al., 2004). This discrepancy may be explained by our shorter time of sleep deprivation as Vyazovskiy et al. used a sleep deprivation protocol of 6 hours. Nonetheless, the fact that spindles were elevated on a local level warrants the consideration that sleep deprivation causes spindles to be less spatially synchronized and possibly not detected from cortical EEG electrodes. Ripple densities after sleep deprivation have not been extensively investigated so far except for one study that found that it did not elevate during recovery sleep in mice that were sleep deprived after a hippocampus-dependent conditioning task as compared to mice that were allowed to sleep immediately after the task (Li et al., 2021). The elevation of ripple densities after sleep deprivation in our study points to a possible homeostatic function. Given that CA1 pyramidal cells do not show similar OFF, or bistable, states as thalamic and cortical neurons do during sleep (Isomura et al., 2006), it is possible that other oscillations than slow waves serve homeostatic functions in the HPC (Miyawaki & Diba, 2016).
On the other hand, the higher event densities after post-learning sleep on the other hand are in line with previous results described for spindles (Eschenko et al., 2006; Fogel & Smith, 2006) and ripples (Eschenko et al., 2008; Li et al., 2021; Ramadan et al., 2009) and further demonstrate the importance of spindles and ripples for memory consolidation.
Furthermore, our results showed a change in the drive of cortico-thalamic slow waves and spindles of hippocampal ripples. The drive of cortical spindles and slow waves on ripples during NREM sleep has been described in humans before (Helfrich et al., 2019). The higher drive after sleep deprivation may be in part be explained through higher synchrony of neuronal ensembles during slow waves, reflected by the higher slope of slow waves after sleep deprivation (Massimini et al., 2009; Tononi & Cirelli, 2006). Thus, increasing synchronous cortical and thalamic neural assemblies may induce a stronger downstream cascade which in turn influences and drives hippocampal ripples more effectively. We theorise, that the higher synchrony slow waves may have an influence on the spindle nesting (Helfrich et al., 2018; Rasch & Born, 2013). The higher drive during post-learning sleep would be consistent with higher mnemonic demands of involved cortical and thalamic areas, which may support the process of memory consolidation and replays of neuronal ensembles (Klinzing et al., 2019). However, the exact initiation of coordinated replays in cortical and hippocampal areas remains to be fully understood. Our results suggest a cortical drive of ripple events, which is consistent with a previous study (Helfrich et al., 2019) and the nesting of ripples in UP states of slow waves and spindle troughs, both of which start before the onset of ripples.

Optogenetic manipulations of Nre during natural NREM sleep showed that Nre plays a key role in coordinating sleep oscillations between Prl and HPC. Particularly, it regulated the coherence of delta frequencies as well as theta and beta frequencies between cortex and the dorsal portion of CA1, which confirms previous findings in anesthetized animals (Hauer et al., 2019; Roy et al., 2017) as well as awake rats during a working memory task (Hallock et al., 2016). Furthermore, our observation confirmed that Nre neurons coordinated phase-locking between hippocampal ripples and cortical slow waves and spindles. Precisely, optogenetic silencing or stimulating did not affect the strength of phase-amplitude coupling (except for vCA1 ripples and slow waves) but rather changed the preferred

phase of ripple occurrence with preserved mean vector length. Additionally, optogenetic silencing or stimulation of Nre increased co-occurrence of cortical slow waves with dCA1 ripples and of cortical spindles with vCA1 ripples, respectively. Additionally, stimulation reduced the drive of slow waves on vCA1 ripples and silencing reduced the drive of slow waves on all ripples.

Despite these changes in cortico-hippocampal communication during NREM sleep, optogenetic manipulation of Nre did not result in any significant changes in sleep-dependent memory performance. This finding contrasts with previous studies assessing the role of Nre in memory consolidation. Troyner et al. (Troyner et al., 2018) observed relatively small but significant levels of generalization in contextual memory performance when silencing Nre with muscimol during the consolidation phase. Similarly, Xu and colleagues reported a strong contextual generalization upon silencing of Nre projections to PFC (Xu & Sudhof, 2013). In the latter study, however, Nre neurons were either chronically silenced using tetrodotoxin *before* fear conditioning or optogenetically stimulated during *acquisition* in a phasic fashion (15 pulses at 30 Hz every 5 seconds). A potential explanation for these discrepancies is the different intervention protocol used in both studies. We used a mild optogenetic perturbation approach based on 20-second-long train of stimulation/silencing every second NREM episode for 4h of NREM sleep in order to restrict perturbation of Nre neural networks that may affect sleep and avoid the triggering of compensatory mechanisms. Thus, Nre cell activities, and associated sleep oscillations, were altered only during a restricted number and duration of NREM sleep episodes (supp. fig. 3d). This contrasts to the methods used in other studies where tetrodotoxin expression in Nre neurons (Xu & Sudhof, 2013), or muscimol infusion in Nre area (Troyner et al., 2018) abolished Nre neuron activity for hours, or an unlimited period of time, respectively, irrespective of the sleep-wake states of the animals after acquisition. Aside from a likely role of Nre cells in cognition during wakefulness, an alternative silencing protocol would possibly involve targeting every UP state of Nre with a closed loops system to disrupt Nre firing before ripple occurrence. Additionally, several studies have demonstrated Nre's involvement in retention of remote memories (Ali et al., 2017; Loureiro et al., 2012; Quet et al., 2020; Troyner et al., 2018). Thus, a promising approach would be to either stimulate or silence Nre neurons during NREM, but also REM, sleep for several days to manipulate the consolidation of remote memories, which may strengthen its implication in the process of '*corticalization'* where memories become independent from the HPC, as proposed by the *systems memory consolidation hypothesis* (Klinzing et al., 2019).

To summarize, our analyses revealed a role of Nre in orchestrating interactions between PFC and HPC during sleep. This interaction is not only crucial for memory consolidation (Klinzing et al., 2019) but also for episodic memory retrieval (Moscovitch et al., 2016; Nadel & Moscovitch, 1997) and working memory (Griffin, 2015; Yoon et al., 2008). Thus, further investigations on the role of Nre neurons in sleep-dependent memory consolidation, or weakening, are warranted. Furthermore, **the clear role** of Nre neurons in mediating prefrontal-hippocampal communication suggested its potential involvement in psychiatric diseases including schizophrenia where disruption of Nre neuronal connections has been reported. In

this context, spatial working memory relies on theta and gamma oscillation coherence between PFC and HPC (Kupferschmidt & Gordon, 2018). Deficits in this cognitive aspect or anatomical defects in medial thalamic regions (Ceyhan et al., 2008; Nopoulos et al., 2001; Takahashi et al., 2008) all have been associated with schizophrenia (Dolleman-van der Weel & Witter, 2020) or dementias.

## Methods

### Animals

We used adult male C57Bl6 mice that were 6-12 weeks old at the time of surgery form Janvier labs, France. Animals were treated according to protocols and guidelines approved by the veterinary office of the Canton of Bern, Switzerland (license no. BE 119/2020). Up until tetrode implantation, mice were housed in groups of 2-5 in IVC cages at constant temperature (22± 1°C), humidity (40-50%) and circadian cycle (12h light-dark cycle with lights on at 08:00). Food and water were provided *ad libitum*. After tetrode implantation, mice were housed individually in custom made hard plastic cages with an open top under the same conditions. After 5 days, mice were chronically tethered to recording cables (and optic fibers, respectively) and mice were given another 10 days of habituation before the start of the experiments. Treatment guidelines and protocols were approved by the Veterinary Office of the Canton of Bern, Switzerland (license number BE129/2020).

### Stereotaxic injection of AAV

At six weeks of age, mice were anesthetized with isoflurane (5% for induction, 1.25-1.75% for maintenance) in oxygen and mounted in a stereotaxic frame (Model 940, David Kopf Instruments). Before incision, saline (10ml/kg) and meloxicam (5mg/kg) were given subcutaneously. The skin above the skull was shaved and aseptically prepared with Betadine, followed by a longitudinal midline incision along the skull from the level of the eyes to the insertion of the trapezoid muscle at the back of the skull. Bregma and the point 5mm caudally to it were aligned to ensure proper positioning of the skull. Injections were done with a Hamilton syringe (7000 series, model 7000.5, 0.5µL volume) and a syringe pump (Pump 11 Elite Nanomite Infusion/Withdrawal Programmable Syringe Pump, Harvard Apparatus). Animals were randomly assigned to receive either AAV2-CamKII-E1fa-ChR2-EYFP, AAV2-CamKII-E1fa-ArchT-EYFP or AAV2-CamKII-E1fa-EYFP. The virus was injected in Nre (-0.66mm AP, 0.3mm ML, -4.29mm DV, 4°, 200nl) according to Paxinos' and Franlin's mouse brain atlas at an injection rate of 50nl/min. After the virus was delivered, the needle was left in the current position for min. 10 minutes to allow diffusion into the brain tissue. After injection, mice were given at least 20 days of recovery before tetrode implantation. All plasmids came either from University of North Carolina Vector Core or University of Zurich Viral Vector Facility.

pAAV.CamKII(1.3).eYFP.WPRE.hGH was a gift from Karl Deisseroth (Addgene plasmid # 105622 ; http://n2t.net/addgene:105622 ; RRID:Addgene_105622)

pAAV-CaMKIIa-hChR2(H134R)-EYFP was a gift from Karl Deisseroth (Addgene plasmid # 26969 ; http://n2t.net/addgene:26969 ; RRID:Addgene_26969) (Lee et al., 2010)

pAAV-CaMKIIa-eArchT3.0-P2A-EGFP-WPRE-hGHpA was a gift from Jonathan Ting (Addgene plasmid # 51110 ; http://n2t.net/addgene:51110 ; RRID:Addgene_51110)

Tetrode implantation

Electrodes for EEG signals and grounding were obtained with stainless steel screws and bare-ended steel wires were used for EMG signals. Tetrodes were made of four strands of 10µm tungsten wire (CFW0010954, California Fine Wire) which were twisted and connected to an electrode interface board by gold pins (EIB-36-PTB, Neuralynx). Anesthesia was induced using isoflurane in oxygen and maintained using a mix of medetomidine (0.27 mg/kg), midazolam (5 mg/kg), fentanyl (0.05 mg/kg). The animals were prepared in the same manner as described above and the screws for the EEG signal ware placed in the skull above the frontal lobe and the parietal lobe, the ground screw was placed above the cerebellum and the EMG wires were sutured to the trapezoid muscle. Tetrodes were implanted into Prl (+1.7mm AP, 0.4mm ML, -2.4mm DV), Nre (-0.66mm AP, 0.4mm ML, -4.38mm DV, 2°), dCA1 (-2.2mm AP, 1.5mm ML, -1.15mm DV) and vCA1 (-2.9mm AP, 3.38mm ML, -4.5mm DV). In the optogenetic experiment, optic fibers of 200µm diameter were additionally implanted in nucleus reuniens via attachment to the respective tetrode in ChR2 and ArchT mice. EYFP control mice were only implanted with the optic fiber. After tetrodes were placed in the right position, they were fixed with Tetric EvoFlow cement by *Ivoclar vivadent*. Once all tetrodes were placed and fixed, the EMG wires and wires attached to the EEG and ground screws were accordingly connected to the interface board and the surgery was finalized by fixing the implant with Paladur methacrylate cement by *Kulzer*. Anesthesia was terminated by injecting Atipamezole, Naloxone and Flumazenil subcutaneously and the mice were given time to recover in their home cage which was placed on a heating mat.

Data acquisition

For all recordings, mice were connected to a tethered, digitizing head stage (RHD2132, Intan Technologies) and recordings were done at 20kHz using an open-source software from Intan Technologies (RHD2000). In the optogenetic experiment, optical fibers were connected to patch cords which were coated with black tubing and the connections were covered in black varnish to avoid disturbing the mice via visual stimulation. First mice underwent recording of baseline sleep (ZT4-ZT-9), followed be sleep deprivation on the following day and fear conditioning one week after sleep deprivation (see below). When sufficient data was acquired in one of the first two experiments, it was omitted.

Sleep deprivation

At the onset of light at 08:00 (ZT0) mice were kept awake for the next 4h by gently handling them when stationary. At ZT 4 the procedure was stopped, and subsequent sleep was recorded from ZT4-ZT9. See supp. fig. 1b and c for power spectral density analysis, showing the increase in delta frequency after sleep deprivation.

Fear conditioning

Before the experiment was started, mice were habituated by gently handling them for 5min on 5 consecutive days. On the first day of the procedure (habituation) at ZT0, a foreign cage with a metal grid as a floor (context A) was wiped with 70% ethanol and the mice were placed in it. The walls were marked with stripes to provide additional contextual information. The mice were first given 3min of time to explore the novel environment, followed

by playing a first auditory stimulus (CS-) consisting of 27 beeps of 50ms duration at 2000 Hz played over 30 seconds for 5 times with a variable interstimulus interval (ISI) between 10s and 30s. Then, a second auditory stimulus (CS+) was played under the same conditions but at 8000Hz. 24h later, acquisition of fear memory was performed by wiping context A with alcohol again and subsequently placing the animals in the same cage with the metal grid. After 3 min, CS+ and CS- were played in an intermixed manner. An unconditional stimulus (US) was paired with CS+ by applying an electric foot shock through the metal grid on the floor at 0.5 mA for 1 second, starting when CS+ ends. Interstimulus interval was set between 15 and 90 seconds. CS-, CS+ paired with US were played 5 times. Another 24h later (recall), a novel cage (context B) was wiped with 1% acetic acid and mice were placed in it. After 3 min of exploration, CS- and CS+ were presented to the mice with the same protocol as during habituation. Approximately 30min later, the mice were placed in context A again to assess contextual fear memory. Freezing behavior was measured as a measure of learning performance. It was scored manually as absence of any movement except breathing. Freezing during context was measured from the end of the first minute onward for two minutes. Freezing to CS+/CS- was measured during the time the tone was playing, and only the first two occurrences of CS+ and CS- were considered. Freezing was quantified as the total time of freezing during the total playing time of the tones, or during the total 2 minutes in context A or B, respectively. If mice generalized in the first series of experiments (Fig.1-3) (i.e., they did not discriminate between CS+ and CS-) they were excluded from the analysis. See supp. fig. 1e and supp. table 1 for results of memory performance.

Optogenetic stimulation protocol

After acquisition, laser pulses between 20-30mW were delivered during every second NREM episode for 4h of NREM sleep. After recall, laser pulses were delivered every 5 minutes for 4 hours of NREM sleep. ChR2 mice and respective EYFP control mice received 5ms pulses à 7Hz for 20 seconds resulting in 140 pulses per stimulation train. ArchT mice and respective EYFP control mice received a single 20-second-long laser pulse for every train. Only trains delivered during NREM were considered for subsequent analysis and only the LFP signals during the stimulation/silencing trains were considered for analysis concerning phase-event coupling, event co-occurrence and phase slope index analysis. The LFP signals were concatenated for coherence measures. The stimulus was not interrupted in case of state transition. After recall, mice underwent another stimulation or silencing protocol to increase the relevant electrophysiological data samples. The stimulation trains were the same, but a train was delivered every 5 min, irrespective of vigilance state for 4h. Only trains occurring during NREM sleep were considered for data analysis.

Sleep scoring

Sleep scoring was performed manually, based on frequency and amplitude characteristics of the EEG and EMG in custom software written in Matlab. NREM sleep was identified by high-amplitude, synchronous activity in the EEG with a delta (0.5- 4 Hz) frequency dominating the signal and low EMG activity, REM by highly synchronous theta (6- 9Hz) especially in the parietal electrode and flat EMG and wake mainly by increased EMG activity. The start of wake was defined as the onset of rapid increase in muscle tone concurrent with a low-amplitude,

high-frequency (>6Hz) EEG, the start of NREM was defined as the first visible slow wave of more than 200µV amplitude and the start of REM was put at the point of a consolidated theta:delta ratio of more than 1.

Single unit activity

Single units were detected using the *Offline sorter Application* by *Plexon Neurotechnology Research Systems* (Version 4.4.1). Raw LFP data was first band-pass filtered (500-4000Hz, Butterworth filter) and a threshold for multiunit activity was set manually. Single unit activity was then extracted using principal components analysis and manually extracting resulting clusters.

Burst firing of single units was defined as a minimum of three consecutive action potentials with ISI <6ms which were preceded by a quiescent hyperpolarized state of at least 50ms. The interburst interval (IBI) was defined as the distance between the centers of two consecutive bursting activities during NREM episodes. IBI histograms during NREM sleep were created for individual units using a 200ms bin width (Gent et al., 2018; Guido et al., 1992).

As described in a previous publication (Gent et al., 2018), the average spike rate during vigilance state was calculated as the total number of action potentials during a state divided by total time spent in that state and reported in Hz for every unit separately. Mean spike rates for each unit during transition from DOWN to UP states were calculated by averaging spike rates during all detected DOWN to UP transitions using a non-overlapping moving window of 10ms. Mean spike rates were then fitted with a Boltzmann sigmoidal curve in GraphPad Prism with the following equation:

$$y = minimum + \frac{maximum - minimum}{1 + \frac{t_{\frac{1}{2}} - x}{slope}}$$

Where *y* is the neuronal spike rate and *x* is time. The half-times of the curves ($t_{½}$) were used for comparison of lag and phase. The slopes of the curve fits at the half-time point were used as a measure of neuronal spiking modulation and therefore synchrony (Vyazovskiy et al., 2009).

Spike rate of Nre cells locked to ripples was calculated using a non-overlapping 50ms window with a total window of 1 second around ripple peak. Increases or decreases around ripple center were tested for significance by comparing the mean spike rate during 150ms around the peak or trough, respectively, to the mean spike rate during a 150ms baseline at the beginning of the 1 second window using a paired signed-rank test.

Preprocessing of LFP data

After acquisition, LFP data was down sampled to 1000Hz and was re-referenced with a common average reference to reduce possible volume conduction. Then, data were z-scored and the EMG trace was subtracted with linear regression.

Slow wave detection

Individual slow waves were detected during NREM sleep in MATLAB using the SWA-MATLAB toolbox (Mensen et al., 2016), with detection parameters adjusted to rodents from settings

described by Panagiotou et al. and Facchin et al. (Facchin et al., 2020; Panagiotou et al., 2017). First, the negative envelope across the LFP signal was calculated, filtered between 0.5 and 4 Hz (Chebyshev Type II filter design), and consecutive zero-crossings were detected. If the duration between successive downward (negative going) zero-crossing and upward zero-crossing was between 100ms and 1s, then the peak negative amplitude was examined and was required to be at least 3 deviations from the median amplitude of all negative peaks in the recording. The amplitude threshold eliminates the potential individual differences of electrode reference type, distance to those references, and electrode depth that would affect the record amplitude. The beginning of the slow wave was marked at the positive to negative zero-crossing before the negative peak and the end of the slow wave was marked at the end of the subsequent positive slope.

Spindle detection

We detected spindles using the wavelet-based method proposed by Wamsley et al. (Wamsley et al., 2012) and Bandarabadi et al. (Bandarabadi et al., 2020). We extracted wavelet energy of the complex frequency B-spline function, which provided the highest normalized power, by considering several criteria. The wavelet energy time series was smoothed using a 200ms Hann window, and a threshold equal to 3SD above the mean was applied to detect potential spindle events. A lower threshold of 1SD above the mean was set to find start and end of detected events. Events shorter than 400ms or longer than 2s were discarded. Using bandpass-filtered LFP signals in the spindle range (9–16 Hz), events with fewer than 5 and more than 30 cycles were discarded as well. To ensure that increases in wavelet energy are spindle specific, and not due to artefacts, we estimated power in the spindle range as well as in 6–8.5 and 16.5–20 Hz frequency bands and discarded those events where power within the spindle band was lower than in the two other bands. We also estimated the central frequency of spindle using the fourier transform. We measured the symmetry of spindles using the position of peak of wavelet energy time-series with regard to the start and end of spindles. The symmetric measure lies between 0 and 1; 0.5 corresponds to complete symmetry, and values lower and higher than 0.5 show a leftward and rightward shift of peak, respectively.

Ripple detection

Ripple detection was based on previously published methods of detecting them (Cheng & Frank, 2008; Navarrete et al., 2016). Data was downsampled to 1000Hz, and band pass filtered by first applying fast fourier transform and subsequently filtered LFP and power of frequencies between 150-250Hz were extracted via inverse fourier transform. Ripples were then detected as events where power surpassed 5SD of the mean power for at least 10ms. Start and end of the ripple were marked at the beginning of the uprising towards the threshold and end of the descend below threshold of the power.

Event densities over time

Event densities for spindles and ripples over time were calculated by cutting out wake and REM episodes and concatenating NREM episodes. Next, the event densities were calculated for 15min bouts over 3h as this was the minimum amount of time all animals slept during the recordings in baseline, rebound and post-learning sleep, thus avoiding higher error margins towards latter parts of recordings.

Co-occurrence measuring

Co-occurrence of slow waves, spindles, and ripples was measured by calculating the average length of spindles and slow waves to determine the window length for co-occurrence. Next the windows for co-occurrence were centered at the middle of slow wave and spindle centers. Co-occurrence was then calculated as a percentage of all detected ripples which occur within the windows.

Phase-amplitude coupling analysis

For the following sections, we performed event-locked cross-frequency analysis. Namely, ripples locked to slow waves and spindles were taken as the events and the LFP data of thalamus, cortex and HPC from -1.25 to 1.25 seconds around the ripples were considered for the following calculations. We used finite-duration impulse response filters (FIR) to band-pass filter the data in the respective frequency range (see above) (forward/backward, filtfilt, Matlab, signal processing toolbox, https://www.mathworks.com/products/signal.html). FIR filters used an order equal to three cycles of the lower cut off frequency. The phase was extracted using Hilbert transform. The peak of a coupled ripple was matched to the corresponding phase value of the slow wave or spindle. Next, a phase-amplitude histogram (PAH) was computed where the phase was divided in 18 bins with each covering 20 degrees and the mean circular vector was calculated. All resulting vectors were tested for non-uniformity with the Rayleigh test for non-uniformity. To estimate if slow waves and spindles drive ripples or vice versa, we calculated the cross-frequency directionality (CFD) on the same events as described above. When two or more ripples occurred within the same slow wave or spindle, that time window was only analyzed once. This measure is based on the phase-slope index (PSI) between the phase of slower oscillations and the power envelope of faster oscillations (Helfrich et al., 2018; H. Jiang et al., 2015). Values above zero indicate that the lower frequency (slow wave or spindle) drives the higher frequency (ripple), while negative values indicate that ripples drive slow waves and spindles. To prove for the statistical significance of CFD, a non-parametric approach based on randomizations was applied. By that we control for multiple comparisons with respect to the multiple frequency pairs included in the analysis (Maris & Oostenveld, 2007). Lastly, a normalization factor was obtained through fitting an exponential decay function to resulting phase slope index values per number of trials and applied to the PSI value of each subject.

Immunohistochemistry and Histology

After all experiments were done, animals were anaesthetized with isoflurane as described above and electric current was sent through two channels of each tetrode (30µA, 5 pulses à 2s) in order to induce gliosis at the spot of tetrode placement. After min. 2h, animals were euthanized with 15mg pentobarbital i.p. and the cardiovascular system was transfused with 30ml of cold, heparinized phosphate buffered saline (PBS), followed by 30ml of 4% Paraformaldehyde (PFA) via puncture in the left ventricle of the heart. Brains were removed and kept in PFA overnight. The next day, they were cryo-protected in 30% sucrose for 48h. Then, they were flash-frozen in 2-methylbutane at approximately -80°C. Next, the brains were cut in 40µm thick sections. To confirm virus transfection, sections were washed in PBS + 0.1% Triton X-100 (PBST) three times for 10min each, blocked by incubation with 4% bovine se-

rum albumin dissolved in PBST for 45mim and subsequently incubated with anti-GFP antibodies (AB_221569) for 24h-48h at 4°C. After that, sections were again washed in PBST (three times à 10min) and then incubated with a secondary antibody (ab150073) that binds to the primary antibody for 1h at room temperature. To confirm tetrode placement, the tetrodes were stained with 1,1'-Dioctadecyl-3,3,3',3'-tetramethyl-indocarbocyanin-perchlorat before implantation. After cutting the brain, sections with visible dye traces were selected and either Nissl-stained or HE-stained to reveal the gliosis.

Statistical methods

We used MATLAB® (R2019b, MathWorks, Natick, MA, USA) and Prism 8 (GraphPad) for all analyses and statistics. The CircStat toolbox was used for circular statistics (no ANOVA tests with multiple comparisons available). To test differences between conditions with circular data, we pooled all obtained phase values for each condition and employed a Parametric Watson-Williams multi-sample test for equal means as a one-way ANOVA test. If the assumptions of the test were not met, a non-parametric multi-sample test for equal medians was employed. Multiple comparisons were subsequently performed by first performing a parametric two-sample test between the experimental condition and the control condition (i.e. baseline sleep in the first experiment or EYFP control in the second experiment). If the test conditions were not met, a non-parametric two-sample test for equal medians was performed. The resulting p-values were then adjusted with Bonferroni correction. No power calculations were performed to determine sample sizes. Data was compared via one-way or two-way ANOVA followed by multiple comparisons tests and *signed rank tests* for non-parametric data, as indicated in the text. Values in the text are reported as mean ± standard error of the means (S.E.M.) unless reported otherwise. Figures were prepared in Adobe Illustrator CC (Adobe).

**Acknowledgments and Disclosures**

We thank Yaroslav Sych and Niccolò Calini for help and support in statistical questions, Simon Ruch for help and support in questions of data preprocessing, Armand Mensen for providing a MATLAB script to score sleep and Rahel Bodmer and Regina Reissmann for help in histological labor. This work was supported by the Inselspital University Hospital Bern, European Research Council (CoG-725850 to A.A.), Swiss National Science Foundation (A.A.), Synapsis Foundation (A.A.), the University of Bern (A.A.), the Graduate School for Cellular and Biomedical Sciences of the University of Bern, and by Swiss National Fund Grant 323530_177976.

Parts of Fig.4 were reprinted from "Asleep mouse", by BioRender.com (2022). Retrieved from https://app.biorender.com/biorender-templates

**Disclosures**

The authors report no potential conflicts of interest.

**Data availability**

All presented data and analysis scripts, including data files, Matlab scripts and functions are available on GitHub.

**List of abbreviations**

| | |
|---|---|
| AP | antero-posterior |
| ArchT | Archaerhodopsin |
| BL | baseline sleep |
| CFD | cross-frequency directionality |
| ChR2 | Channelrhodopsine-2 |
| CS- | conditional stimulus, not paired with US |
| CS+ | conditional stimulus, paired with US |
| dCA1 | dorsal CA1 |
| DV | dorso-ventral |
| EEG | electroencephalogram |
| EMG | electromyogram |
| EYFP | Enhanced yellow fluorescent protein |
| FIR filter | finite impulse response filter |
| LFP | local field potential |
| PL | post-learning sleep |
| ML | medio-lateral |
| mPFC | medial prefrontal cortex |
| Nre | Thalamic nucleus reuniens |
| PAH | phase amplitude histogram |
| PBS | phosphate buffered saline |
| PBST | phosphate buffered saline and triton X-100 |
| PFA | paraformaldehyde |

| | |
|---|---|
| PFC | prefrontal cortex |
| Prl | prelimbic cortex |
| PSI | phase slope index |
| Reb | rebounds sleep |
| S.E.M. | standard error of the means |
| US | unconditional stimulus |
| vCA1 | ventral CA1 |
| ZT | Zeitgeber |

**References**


Adamantidis, A. R., Gutierrez Herrera, C., & Gent, T. C. (2019). Oscillating circuitries in the sleeping brain. *Nature Reviews Neuroscience*, *20*(12), 746–762. https://doi.org/10.1038/s41583-019-0223-4

Aime, M., Augusto, E., Kouskoff, V., Campelo, T., Martin, C., Humeau, Y., Chenouard, N., & Gambino, F. (2020). The integration of Gaussian noise by long-range amygdala inputs in frontal circuit promotes fear learning in mice. *ELife*, *9*, e62594. https://doi.org/10.7554/eLife.62594

Ali, M., Cholvin, T., Muller, M. A., Cosquer, B., Kelche, C., Cassel, J.-C., & Pereira de Vasconcelos, A. (2017). Environmental enrichment enhances systems-level consolidation of a spatial memory after lesions of the ventral midline thalamus. *Neurobiology of Learning and Memory*, *141*, 108–123. https://doi.org/10.1016/j.nlm.2017.03.021

Angulo-Garcia, D., Ferraris, M., Ghestem, A., Nallet-Khosrofian, L., Bernard, C., & Quilichini, P. P. (2020). Cell Assemblies in the Cortico-Hippocampal-Reuniens Network during Slow Oscillations. *The Journal of Neuroscience*, *40*(43), 8343–8354. https://doi.org/10.1523/JNEUROSCI.0571-20.2020

Apergis-Schoute, J., Pinto, A., & Paré, D. (2006). Ultrastructural organization of medial prefrontal inputs to the rhinal cortices. *European Journal of Neuroscience*, *24*(1), 135–144. https://doi.org/10.1111/j.1460-9568.2006.04894.x

Bandarabadi, M., Herrera, C. G., Gent, T. C., Bassetti, C., Schindler, K., & Adamantidis, A. R. (2020). A role for spindles in the onset of rapid eye movement sleep. *Nature Communications*, *11*(1), 5247. https://doi.org/10.1038/s41467-020-19076-2

Banks, P. J., Warburton, E. C., & Bashir, Z. I. (2021). Plasticity in Prefrontal Cortex Induced by Coordinated Synaptic Transmission Arising from Reuniens/Rhomboid Nuclei and Hippocampus. *Cerebral Cortex Communications*, *2*(2), tgab029. https://doi.org/10.1093/texcom/tgab029

Buzsáki, G. (2015). Hippocampal sharp wave-ripple: A cognitive biomarker for episodic memory and planning. *Hippocampus*, *25*(10), 1073–1188. https://doi.org/10.1002/hipo.22488

Cassel, J. C., Pereira de Vasconcelos, A., Loureiro, M., Cholvin, T., Dalrymple-Alford, J. C., & Vertes, R. P. (2013). The reuniens and rhomboid nuclei: Neuroanatomy, electrophysiological characteristics and behavioral implications. *Prog Neurobiol*, *111*, 34–52. https://doi.org/10.1016/j.pneurobio.2013.08.006

Ceyhan, M., Adapınar, B., Aksaray, G., Ozdemir, F., & Colak, E. (2008). Absence and size of *massa intermedia* in patients with schizophrenia and bipolar disorder. *Acta Neuropsychiatrica*, *20*(4), 193–198. https://doi.org/10.1111/j.1601-5215.2008.00296.x

Cheng, S., & Frank, L. M. (2008). New Experiences Enhance Coordinated Neural Activity in the Hippocampus. *Neuron*, *57*(2), 303–313. https://doi.org/10.1016/j.neuron.2007.11.035

Clemens, Z., Molle, M., Eross, L., Barsi, P., Halasz, P., & Born, J. (2007). Temporal coupling of parahippocampal ripples, sleep spindles and slow oscillations in humans. *Brain*, *130*(Pt 11), 2868–2878. https://doi.org/10.1093/brain/awm146

Clemens, Z., Molle, M., Eross, L., Jakus, R., Rasonyi, G., Halasz, P., & Born, J. (2011). Fine-tuned coupling between human parahippocampal ripples and sleep spindles. *Eur J Neurosci*, *33*(3), 511–520. https://doi.org/10.1111/j.1460-9568.2010.07505.x

Crunelli, V., Lőrincz, M. L., Connelly, W. M., David, F., Hughes, S. W., Lambert, R. C., Lerescche, N., & Errington, A. C. (2018). Dual function of thalamic low-vigilance state oscillations: Rhythm-regulation and plasticity. *Nature Reviews Neuroscience*, *19*(2), 107–118. https://doi.org/10.1038/nrn.2017.151

Davoodi, F. G., Motamedi, F., Akbari, E., Ghanbarian, E., & Jila, B. (2011). Effect of reversible inactivation of reuniens nucleus on memory processing in passive avoidance task. *Behavioural Brain Research*, *221*(1), 1–6. https://doi.org/10.1016/j.bbr.2011.02.020

Diekelmann, S., & Born, J. (2010). The memory function of sleep. *Nature Reviews Neuroscience*, *11*, 114–126. https://doi.org/10.1038/nrn2762

Dijk, D.-J., Hayes, B., & Czeisler, C. A. (1993). Dynamics of electroencephalographic sleep spindles and slow wave activity in men: Effect of sleep deprivation. *Brain Research*, *626*(1–2), 190–199. https://doi.org/10.1016/0006-8993(93)90579-C

Dolleman-van der Weel, M. J., Griffin, A. L., Ito, H. T., Shapiro, M. L., Witter, M. P., Vertes, R. P., & Allen, T. A. (2019). The nucleus reuniens of the thalamus sits at the nexus of a hippocampus and medial prefrontal cortex circuit enabling memory and behavior. *Learning & Memory*, *26*(7), 191–205. https://doi.org/10.1101/lm.048389.118

Dolleman-van der Weel, M. J., & Witter, M. P. (2020). The thalamic midline nucleus reuniens: Potential relevance for schizophrenia and epilepsy. *Neuroscience & Biobehavioral Reviews*, *119*, 422–439. https://doi.org/10.1016/j.neubiorev.2020.09.033

Duvarci, S., & Pare, D. (2014). Amygdala Microcircuits Controlling Learned Fear. *Neuron*, *82*(5), 966–980. https://doi.org/10.1016/j.neuron.2014.04.042

Eschenko, O., Molle, M., Born, J., & Sara, S. J. (2006). Elevated Sleep Spindle Density after Learning or after Retrieval in Rats. *Journal of Neuroscience*, *26*(50), 12914–12920. https://doi.org/10.1523/JNEUROSCI.3175-06.2006

Eschenko, O., Ramadan, W., Mölle, M., Born, J., & Sara, S. J. (2008). Sustained increase in hippocampal sharp-wave ripple activity during slow-wave sleep after learning. *Learning & Memory*, *15*(4), 222–228. https://doi.org/10.1101/lm.726008

Facchin, L., Schöne, C., Mensen, A., Bandarabadi, M., Pilotto, F., Saxena, S., Libourel, P. A., Bassetti, C. L. A., & Adamantidis, A. R. (2020). Slow Waves Promote Sleep-Dependent Plasticity and Functional Recovery after Stroke. *The Journal of Neuroscience*, *40*(45), 8637–8651. https://doi.org/10.1523/JNEUROSCI.0373-20.2020

Fanselow, M. S., & Dong, H. W. (2010). Are the dorsal and ventral hippocampus functionally distinct structures? *Neuron*, *65*(1), 7–19. https://doi.org/10.1016/j.neuron.2009.11.031

Ferraris, M., Ghestem, A., Vicente, A. F., Nallet-Khosrofian, L., Bernard, C., & Quilichini, P. P. (2018). The Nucleus Reuniens Controls Long-Range Hippocampo-Prefrontal Gamma Synchronization during Slow Oscillations. *J Neurosci*, *38*(12), 3026–3038. https://doi.org/10.1523/JNEUROSCI.3058-17.2018

Fogel, S. M., & Smith, C. T. (2006). Learning-dependent changes in sleep spindles and Stage 2 sleep. *Journal of Sleep Research*, *15*(3), 250–255. https://doi.org/10.1111/j.1365-2869.2006.00522.x

Gabbott, P., Headlam, A., & Busby, S. (2002). Morphological evidence that CA1 hippocampal afferents monosynaptically innervate PV-containing neurons and NADPH-diaphorase reactive cells in the medial prefrontal cortex (Areas 25/32) of the rat. *Brain Research*, *946*(2), 314–322. https://doi.org/10.1016/S0006-8993(02)02487-3

Gais, S., Mölle, M., Helms, K., & Born, J. (2002). Learning-Dependent Increases in Sleep Spindle Density. *The Journal of Neuroscience*, *22*(15), 6830–6834. https://doi.org/10.1523/JNEUROSCI.22-15-06830.2002

Gent, T. C., Bandarabadi, M., Herrera, C. G., & Adamantidis, A. R. (2018). Thalamic dual control of sleep and wakefulness. *Nature Neuroscience*, *21*(7), 974–984. https://doi.org/10.1038/s41593-018-0164-7

Girardeau, G., Benchenane, K., Wiener, S. I., Buzsáki, G., & Zugaro, M. B. (2009). Selective suppression of hippocampal ripples impairs spatial memory. *Nature Neuroscience*, *12*(10), 1222–1223. https://doi.org/10.1038/nn.2384

Griffin, A. L. (2015). Role of the thalamic nucleus reuniens in mediating interactions between the hippocampus and medial prefrontal cortex during spatial working memory. *Frontiers in Systems Neuroscience*, *9*. https://doi.org/10.3389/fnsys.2015.00029

Guido, W., Lu, S. M., & Sherman, S. M. (1992). Relative contributions of burst and tonic responses to the receptive field properties of lateral geniculate neurons in the cat. *Journal of Neurophysiology*, *68*(6), 2199–2211. https://doi.org/10.1152/jn.1992.68.6.2199

Hallock, H. L., Wang, A., & Griffin, A. L. (2016). Ventral Midline Thalamus Is Critical for Hippocampal-Prefrontal Synchrony and Spatial Working Memory. *Journal of Neuroscience*, *36*(32), 8372–8389. https://doi.org/10.1523/JNEUROSCI.0991-16.2016

Hallock, H. L., Wang, A., Shaw, C. L., & Griffin, A. L. (2013). Transient inactivation of the thalamic nucleus reuniens and rhomboid nucleus produces deficits of a working-memory dependent tactile-visual conditional discrimination task. *Behavioral Neuroscience*, *127*(6), 860–866. https://doi.org/10.1037/a0034653

Hauer, B. E., Pagliardini, S., & Dickson, C. T. (2019). The Reuniens Nucleus of the Thalamus Has an Essential Role in Coordinating Slow-Wave Activity between Neocortex and Hippocampus. *Eneuro*, *6*(5), ENEURO.0365-19.2019. https://doi.org/10.1523/ENEURO.0365-19.2019

Helfrich, R. F., Lendner, J. D., Mander, B. A., Guillen, H., Paff, M., Mnatsakanyan, L., Vadera, S., Walker, M. P., Lin, J. J., & Knight, R. T. (2019). Bidirectional prefrontal-hippocampal dynamics organize information transfer during sleep in humans. *Nature Communications*, *10*(1), 3572. https://doi.org/10.1038/s41467-019-11444-x

Helfrich, R. F., Mander, B. A., Jagust, W. J., Knight, R. T., & Walker, M. P. (2018). Old Brains Come Uncoupled in Sleep: Slow Wave-Spindle Synchrony, Brain Atrophy, and Forgetting. *Neuron*, *97*(1), 221-230.e4. https://doi.org/10.1016/j.neuron.2017.11.020

Isomura, Y., Sirota, A., Özen, S., Montgomery, S., Mizuseki, K., Henze, D. A., & Buzsáki, G. (2006). Integration and Segregation of Activity in Entorhinal-Hippocampal Subregions by Neocortical Slow Oscillations. *Neuron*, *52*(5), 871–882. https://doi.org/10.1016/j.neuron.2006.10.023

Jiang, X., Gonzalez-Martinez, J., & Halgren, E. (2019). Coordination of Human Hippocampal Sharpwave Ripples during NREM Sleep with Cortical Theta Bursts, Spindles, Downstates, and Upstates. *The Journal of Neuroscience*, *39*(44), 8744–8761. https://doi.org/10.1523/JNEUROSCI.2857-18.2019

Jimenez, J. C., Berry, J. E., Lim, S. C., Ong, S. K., Kheirbek, M. A., & Hen, R. (2020). Contextual fear memory retrieval by correlated ensembles of ventral CA1 neurons. *Nature Communications*, *11*(1), 3492. https://doi.org/10.1038/s41467-020-17270-w

Jin, J., & Maren, S. (2015). Prefrontal-Hippocampal Interactions in Memory and Emotion. *Frontiers in Systems Neuroscience*, *9*. https://www.frontiersin.org/article/10.3389/fnsys.2015.00170

Klinzing, J. G., Niethard, N., & Born, J. (2019). Mechanisms of systems memory consolidation during sleep. *Nature Neuroscience*, *22*(10), 1598–1610. https://doi.org/10.1038/s41593-019-0467-3

Knoblauch, V., Martens, W. L. J., Wirz-Justice, A., & Cajochen, C. (2003). Human sleep spindle characteristics after sleep deprivation. *Clinical Neurophysiology*, *114*(12), 2258–2267. https://doi.org/10.1016/S1388-2457(03)00238-4

Kupferschmidt, D. A., & Gordon, J. A. (2018). The dynamics of disordered dialogue: Prefrontal, hippocampal and thalamic miscommunication underlying working memory deficits in schizophrenia. *Brain and Neuroscience Advances*, *2*, 239821281877182. https://doi.org/10.1177/2398212818771821

Latchoumane, C. V., Ngo, H. V., Born, J., & Shin, H. S. (2017). Thalamic Spindles Promote Memory Formation during Sleep through Triple Phase-Locking of Cortical, Thalamic, and Hippocampal Rhythms. *Neuron*, *95*(2), 424-435 e6. https://doi.org/10.1016/j.neuron.2017.06.025

Layfield, D. M., Patel, M., Hallock, H., & Griffin, A. L. (2015). Inactivation of the nucleus reuniens/rhomboid causes a delay-dependent impairment of spatial working memory. *Neurobiology of Learning and Memory*, *125*, 163–167. https://doi.org/10.1016/j.nlm.2015.09.007

Lee, J. H., Durand, R., Gradinaru, V., Zhang, F., Goshen, I., Kim, D.-S., Fenno, L. E., Ramakrishnan, C., & Deisseroth, K. (2010). Global and local fMRI signals driven by neurons defined optogenetically by type and wiring. *Nature*, *465*(7299), 788–792. https://doi.org/10.1038/nature09108

Li, R.-R., Yan, J., Chen, H., Zhang, W.-W., Hu, Y.-B., Zhang, J., Hu, Z.-A., Xiong, Y., Yao, Z.-X., & Hu, B. (2021). Sleep Deprivation Impairs Learning-Induced Increase in Hippocampal Sharp Wave Ripples and Associated Spike Dynamics during Recovery Sleep. *Cerebral Cortex*, bhab247. https://doi.org/10.1093/cercor/bhab247

Likhtik, E., & Paz, R. (2015). Amygdala–prefrontal interactions in (mal)adaptive learning. *Trends in Neurosciences*, *38*(3), 158–166. https://doi.org/10.1016/j.tins.2014.12.007

Lin, Y.-J., Chiou, R.-J., & Chang, C. (2020). The Reuniens and Rhomboid Nuclei Are Required for Acquisition of Pavlovian Trace Fear Conditioning in Rats. *Eneuro*, *7*(3), ENEURO.0106-20.2020. https://doi.org/10.1523/ENEURO.0106-20.2020

Loureiro, M., Cholvin, T., Lopez, J., Merienne, N., Latreche, A., Cosquer, B., Geiger, K., Kelche, C., Cassel, J. C., & Pereira de Vasconcelos, A. (2012). The ventral midline thalamus (reuniens and rhomboid nuclei) contributes to the persistence of spatial memory in rats. *J Neurosci*, *32*(29), 9947–9959. https://doi.org/10.1523/JNEUROSCI.0410-12.2012

Maingret, N., Girardeau, G., Todorova, R., Goutierre, M., & Zugaro, M. (2016). Hippocampo-cortical coupling mediates memory consolidation during sleep. *Nat Neurosci*, *19*(7), 959–964. https://doi.org/10.1038/nn.4304

Maisson, D. J., Gemzik, Z. M., & Griffin, A. L. (2018). Optogenetic suppression of the nucleus reuniens selectively impairs encoding during spatial working memory. *Neurobiol Learn Mem*, *155*, 78–85. https://doi.org/10.1016/j.nlm.2018.06.010

Maris, E., & Oostenveld, R. (2007). Nonparametric statistical testing of EEG- and MEG-data. *Journal of Neuroscience Methods*, *164*(1), 177–190. https://doi.org/10.1016/j.jneumeth.2007.03.024

Marr, D., Willshaw, D., & McNaughton, B. (1991). Simple Memory: A Theory for Archicortex. In L. Vaina (Ed.), *From the Retina to the Neocortex* (pp. 59–128). Birkhäuser Boston. https://doi.org/10.1007/978-1-4684-6775-8_5

Massimini, M., Tononi, G., & Huber, R. (2009). Slow waves, synaptic plasticity and information processing: Insights from transcranial magnetic stimulation and high-density EEG experiments. *European Journal of Neuroscience*, *29*(9), 1761–1770. https://doi.org/10.1111/j.1460-9568.2009.06720.x

McCormick, D. A., & Bal, T. (1997). SLEEP AND AROUSAL: Thalamocortical Mechanisms. *Annual Review of Neuroscience*, *20*(1), 185–215. https://doi.org/10.1146/annurev.neuro.20.1.185

Mei, H., Logothetis, N. K., & Eschenko, O. (2018). The activity of thalamic nucleus reuniens is critical for memory retrieval, but not essential for the early phase of 'off-line' consolidation. *Learn Mem*, *25*(3), 129–137. https://doi.org/10.1101/lm.047134.117

Mensen, A., Riedner, B., & Tononi, G. (2016). Optimizing detection and analysis of slow waves in sleep EEG. *Journal of Neuroscience Methods*, *274*, 1–12. https://doi.org/10.1016/j.jneumeth.2016.09.006

Miyawaki, H., & Diba, K. (2016). Regulation of Hippocampal Firing by Network Oscillations during Sleep. *Current Biology*, *26*(7), 893–902. https://doi.org/10.1016/j.cub.2016.02.024

Mölle, M., Eschenko, O., Gais, S., Sara, S. J., & Born, J. (2009). The influence of learning on sleep slow oscillations and associated spindles and ripples in humans and rats. *European Journal of Neuroscience*, *29*(5), 1071–1081. https://doi.org/10.1111/j.1460-9568.2009.06654.x

Moscovitch, M., Cabeza, R., Winocur, G., & Nadel, L. (2016). Episodic Memory and Beyond: The Hippocampus and Neocortex in Transformation. *Annual Review of Psychology*, *67*(1), 105–134. https://doi.org/10.1146/annurev-psych-113011-143733

Nadel, L., & Moscovitch, M. (1997). Memory consolidation, retrograde amnesia and the hippocampal complex. *Current Opinion in Neurobiology*, *7*(2), 217–227. https://doi.org/10.1016/S0959-4388(97)80010-4

Navarrete, M., Alvarado-Rojas, C., Le Van Quyen, M., & Valderrama, M. (2016). RIPPLELAB: A Comprehensive Application for the Detection, Analysis and Classification of High Frequency Oscillations in Electroencephalographic Signals. *PLOS ONE*, *11*(6), e0158276. https://doi.org/10.1371/journal.pone.0158276

Nopoulos, P. C., Rideout, D., Crespo-Facorro, B., & Andreasen, N. C. (2001). Sex differences in the absence of massa intermedia in patients with schizophrenia versus healthy controls. *Schizophrenia Research*, *48*(2–3), 177–185. https://doi.org/10.1016/S0920-9964(00)00067-0

Ornelas, L. C., Van Voorhies, K., & Besheer, J. (2021). The role of the nucleus reuniens in regulating contextual conditioning with the predator odor TMT in female rats. *Psychopharmacology*. https://doi.org/10.1007/s00213-021-05957-x

Oyanedel, C. N., Durán, E., Niethard, N., Inostroza, M., & Born, J. (2020). Temporal associations between sleep slow oscillations, spindles and ripples. *European Journal of Neuroscience*, *52*(12), 4762–4778. https://doi.org/10.1111/ejn.14906

Panagiotou, M., Vyazovskiy, V. V., Meijer, J. H., & Deboer, T. (2017). Differences in electroencephalographic non-rapid-eye movement sleep slow-wave characteristics between young and old mice. *Scientific Reports*, *7*(1), 43656. https://doi.org/10.1038/srep43656

Phillips, K. G., Bartsch, U., McCarthy, A. P., Edgar, D. M., Tricklebank, M. D., Wafford, K. A., & Jones, M. W. (2012). Decoupling of Sleep-Dependent Cortical and Hippocampal Interactions in a Neurodevelopmental Model of Schizophrenia. *Neuron*, *76*(3), 526–533. https://doi.org/10.1016/j.neuron.2012.09.016

Puentes-Mestril, C., & Aton, S. J. (2017). Linking Network Activity to Synaptic Plasticity during Sleep: Hypotheses and Recent Data. *Frontiers in Neural Circuits*, *11*. https://doi.org/10.3389/fncir.2017.00061

Quet, E., Majchrzak, M., Cosquer, B., Morvan, T., Wolff, M., Cassel, J.-C., Pereira de Vasconcelos, A., & Stéphan, A. (2020). The reuniens and rhomboid nuclei are necessary for contextual fear memory persistence in rats. *Brain Structure and Function*, *225*(3), 955–968. https://doi.org/10.1007/s00429-020-02048-z

Ramadan, W., Eschenko, O., & Sara, S. J. (2009). Hippocampal sharp wave/ripples during sleep for consolidation of associative memory. *PLoS One*, *4*(8), e6697. https://doi.org/10.1371/journal.pone.0006697

Ramanathan, K. R., & Maren, S. (2019). Nucleus reuniens mediates the extinction of contextual fear conditioning. *Behavioural Brain Research*, *374*, 112114. https://doi.org/10.1016/j.bbr.2019.112114

Ramanathan, K. R., Ressler, R. L., Jin, J., & Maren, S. (2018). Nucleus Reuniens Is Required for Encoding and Retrieving Precise, Hippocampal-Dependent Contextual Fear Memories in Rats. *The Journal of Neuroscience*, *38*(46), 9925–9933. https://doi.org/10.1523/JNEUROSCI.1429-18.2018

Rasch, B., & Born, J. (2013). About Sleep's Role in Memory. *Physiological Reviews*, *93*(2), 681–766. https://doi.org/10.1152/physrev.00032.2012

Roy, A., Svensson, F. P., Mazeh, A., & Kocsis, B. (2017). Prefrontal-hippocampal coupling by theta rhythm and by 2-5 Hz oscillation in the delta band: The role of the nucleus reuniens of the thalamus. *Brain Struct Funct*, *222*(6), 2819–2830. https://doi.org/10.1007/s00429-017-1374-6

Schwabe, M. R., Lincoln, C. M., Ivers, M. M., & Frick, K. M. (2021). Chemogenetic inactivation of the nucleus reuniens impairs object placement memory in female mice. *Neurobiology of Learning and Memory*, *185*, 107521. https://doi.org/10.1016/j.nlm.2021.107521

Siapas, A. G., & Wilson, M. A. (1998). Coordinated Interactions between Hippocampal Ripples and Cortical Spindles during Slow-Wave Sleep. *Neuron*, *21*(5), 1123–1128. https://doi.org/10.1016/S0896-6273(00)80629-7

Sierra-Mercado, D., Padilla-Coreano, N., & Quirk, G. J. (2011). Dissociable roles of prelimbic and infralimbic cortices, ventral hippocampus, and basolateral amygdala in the expression and extinction of conditioned fear. *Neuropsychopharmacology*, *36*(2), 529–538. https://doi.org/10.1038/npp.2010.184

Sirota, A., & Buzsaki, G. (2005). Interaction between neocortical and hippocampal networks via slow oscillations. *Thalamus Relat Syst*, *3*(4), 245–259. https://doi.org/10.1017/S1472928807000258

Sirota, A., Csicsvari, J., Buhl, D., & Buzsáki, G. (2003). Communication between neocortex and hippocampus during sleep in rodents. *PNAS*, *100*(4). https://doi.org/10.1073/pnas.0437938100

Sotres-Bayon, F., Sierra-Mercado, D., Pardilla-Delgado, E., & Quirk, G. J. (2012). Gating of fear in prelimbic cortex by hippocampal and amygdala inputs. *Neuron*, *76*(4), 804–812. https://doi.org/10.1016/j.neuron.2012.09.028

Staresina, B. P., Bergmann, T. O., Bonnefond, M., van der Meij, R., Jensen, O., Deuker, L., Elger, C. E., Axmacher, N., & Fell, J. (2015). Hierarchical nesting of slow oscillations, spindles and ripples in the human hippocampus during sleep. *Nat Neurosci*, *18*(11), 1679–1686. https://doi.org/10.1038/nn.4119

Steriade, M. (2000). Corticothalamic resonance, states of vigilance and mentation. *Neuroscience*, *101*(2), 243–276. https://doi.org/10.1016/S0306-4522(00)00353-5

Steriade, M., Nunez, A., & Amzica, F. (1993). A novel slow (< 1 Hz) oscillation of neocortical neurons in vivo: Depolarizing and hyperpolarizing components. *The Journal of Neuroscience*, *13*(8), 3252–3265. https://doi.org/10.1523/JNEUROSCI.13-08-03252.1993

Takahashi, T., Suzuki, M., Zhou, S.-Y., Nakamura, K., Tanino, R., Kawasaki, Y., Seal, M. L., Seto, H., & Kurachi, M. (2008). Prevalence and length of the adhesio interthalamica in schizophrenia spectrum disorders. *Psychiatry Research: Neuroimaging*, *164*(1), 90–94. https://doi.org/10.1016/j.pscychresns.2008.03.001

Thierry, A.-M., Gioanni, Y., Dégénétais, E., & Glowinski, J. (2000). Hippocampo-prefrontal cortex pathway: Anatomical and electrophysiological characteristics. *Hippocampus*, *10*(4), 411–419. https://doi.org/10.1002/1098-1063(2000)10:4<411::AID-HIPO7>3.0.CO;2-A

Tononi, G., & Cirelli, C. (2006). Sleep function and synaptic homeostasis. *Sleep Medicine Reviews*, *10*(1), 49–62. https://doi.org/10.1016/j.smrv.2005.05.002

Tononi, G., & Cirelli, C. (2014). Sleep and the Price of Plasticity: From Synaptic and Cellular Homeostasis to Memory Consolidation and Integration. *Neuron*, *81*(1), 12–34. https://doi.org/10.1016/j.neuron.2013.12.025.

Troyner, F., & Bertoglio, L. J. (2020). Thalamic nucleus reuniens regulates fear memory destabilization upon retrieval. *Neurobiology of Learning and Memory*, *175*, 107313. https://doi.org/10.1016/j.nlm.2020.107313

Troyner, F., & Bertoglio, L. J. (2021). Nucleus reuniens of the thalamus controls fear memory reconsolidation. *Neurobiology of Learning and Memory*, *177*, 107343. https://doi.org/10.1016/j.nlm.2020.107343

Troyner, F., Bicca, M. A., & Bertoglio, L. J. (2018). Nucleus reuniens of the thalamus controls fear memory intensity, specificity and long-term maintenance during consolidation. *Hippocampus*, *28*(8), 602–616. https://doi.org/10.1002/hipo.22964

Varela, C., Kumar, S., Yang, J. Y., & Wilson, M. A. (2014). Anatomical substrates for direct interactions between hippocampus, medial prefrontal cortex, and the thalamic nucleus reuniens. *Brain Struct Funct*, *219*(3), 911–929. https://doi.org/10.1007/s00429-013-0543-5

Vidal-Gonzalez, I., Vidal-Gonzalez, B., Rauch, S. L., & Quirk, G. J. (2006). Microstimulation reveals opposing influences of prelimbic and infralimbic cortex on the expression of conditioned fear. *Learning & Memory*, *13*(6), 728–733. https://doi.org/10.1101/lm.306106

Vyazovskiy, V. V., Achermann, P., & Borbély, A. A. (2004). The dynamics of spindles and EEG slow-wave activity in NREM sleep in mice. *Archives Italiennes de Biologie*, *142*(4).

Vyazovskiy, V. V., Olcese, U., Lazimy, Y. M., Faraguna, U., Esser, S. K., Williams, J. C., Cirelli, C., & Tononi, G. (2009). Cortical firing and sleep homeostasis. *Neuron*, *63*(6), 865–878. https://doi.org/10.1016/j.neuron.2009.08.024

Wamsley, E. J., Tucker, M. A., Shinn, A. K., Ono, K. E., McKinley, S. K., Ely, A. V., Goff, D. C., Stickgold, R., & Manoach, D. S. (2012). Reduced Sleep Spindles and Spindle Coherence in Schizophrenia: Mechanisms of Impaired Memory Consolidation? *Biological Psychiatry*, *71*(2), 154–161. https://doi.org/10.1016/j.biopsych.2011.08.008

Xu, W., & Sudhof, T. C. (2013). A neural circuit for memory specificity and generalization. *Science*, *339*(6125), 1290–1295. https://doi.org/10.1126/science.1229534

Yoon, T., Okada, J., Jung, M. W., & Kim, J. J. (2008). Prefrontal cortex and hippocampus subserve different components of working memory in rats. *Learning & Memory*, *15*(3), 97–105. https://doi.org/10.1101/lm.850808

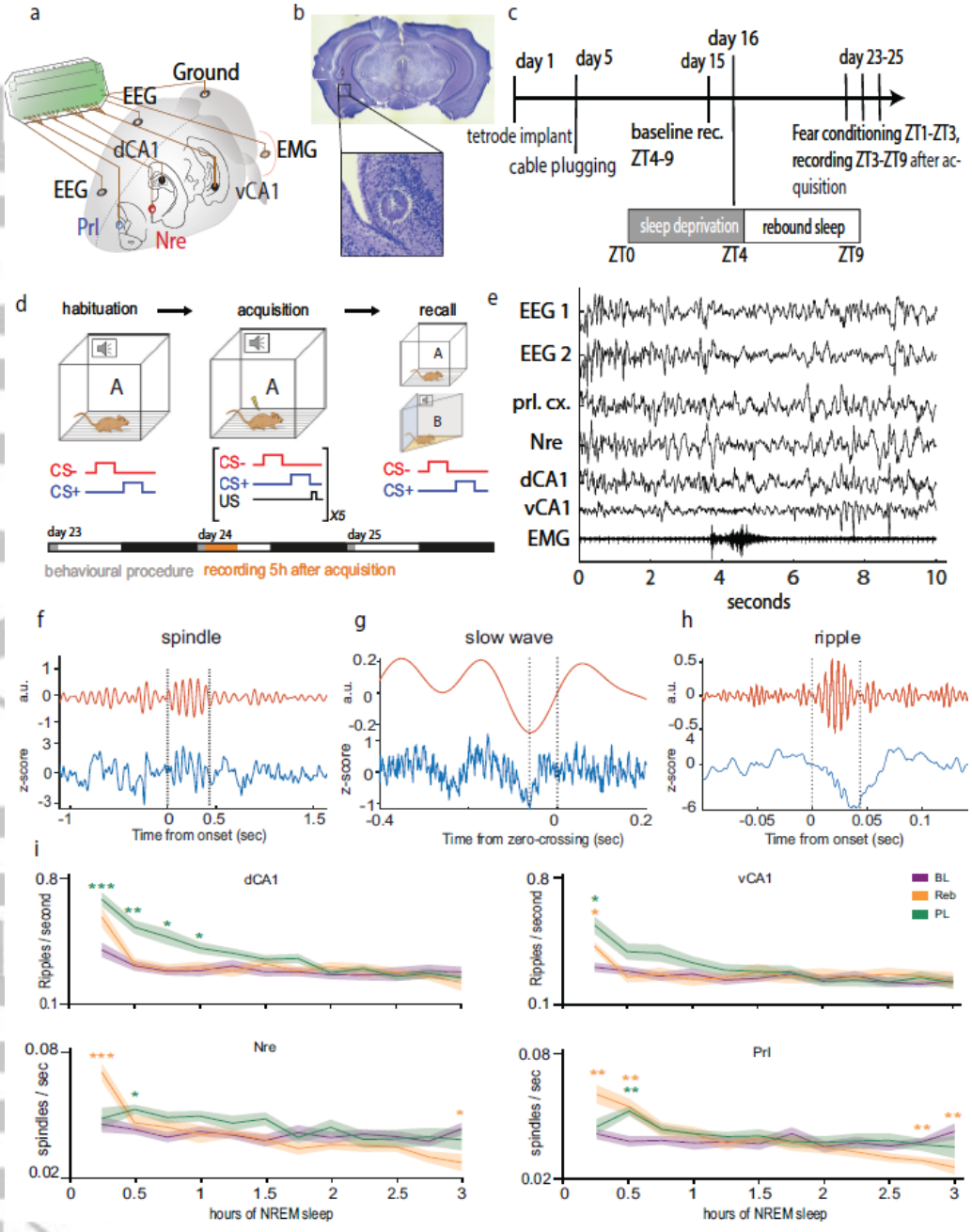


**Figure 1: Experimental design and event detection.**

a) Schematic showing tetrode and electrode placement. Tetrodes were placed in prelimbic cortex (Prl), nucleus reuniens of the thalamus (Nre), dorsal CA1 (dCA1) and ventral CA1 (vCA1).

b) Example of gliosis marking tetrode placement in vCA1 after electric current was driven through the tetrode.

c) Timeline of the experimental procedure marking days of tetrode and electrode implantation, tethering to recording cables, baseline sleep recording, sleep deprivation and fear conditioning.

d) Schematic showing the fear conditioning procedure over three days: mice were first habituated to context A, CS- and CS+, followed by acquisition of fear memory and later recall of fear memory.

e) Example trace of EEG, LFP and EMG recordings, showing a period of NREM sleep with a short arousal approximately at second 4.

f) Example of a detected spindle during NREM sleep. Top shows the filtered trace (9-16Hz, artificial unit) and bottom shows the raw LFP trace (z-scored).

g) Example of a slow wave centered at the negative peak and the following zero-crossing with the filtered trace at the top (0.5-4Hz, artificial unit) and raw LFP trace at the bottom (z-scored).

h) Example of a hippocampal ripple with filtered trace (150-250Hz, artificial unit) on the top and raw LFP trace at the bottom (z-scored).

i) Time-course of ripples and spindles +/- S.E.M. during NREM sleep (NREM sleep bouts were concatenated and cut to 3h, as the minimum duration of sleep for all animals across conditions) in dCA1 ripples (n= 11 in BL, n= 8 in Reb, n= 9 in PL; top left), vCA1 ripples (n= 8 in BL, n= 8 in Reb, n= 8 in PL; top right), Nre spindles (n= 14 in BL, n= 11 in Reb, n= 9 in PL; bottom left) and Prl spindles (n= 14 in BL, n= 11 in Reb, n= 8 in PL; bottom right) during baseline (BL), rebound sleep (Reb) and post-learning sleep (PL). *P<0.05, **P<0.01, ***P<0.0001 using two-way ANOVA with Dunnett's multiple comparisons.

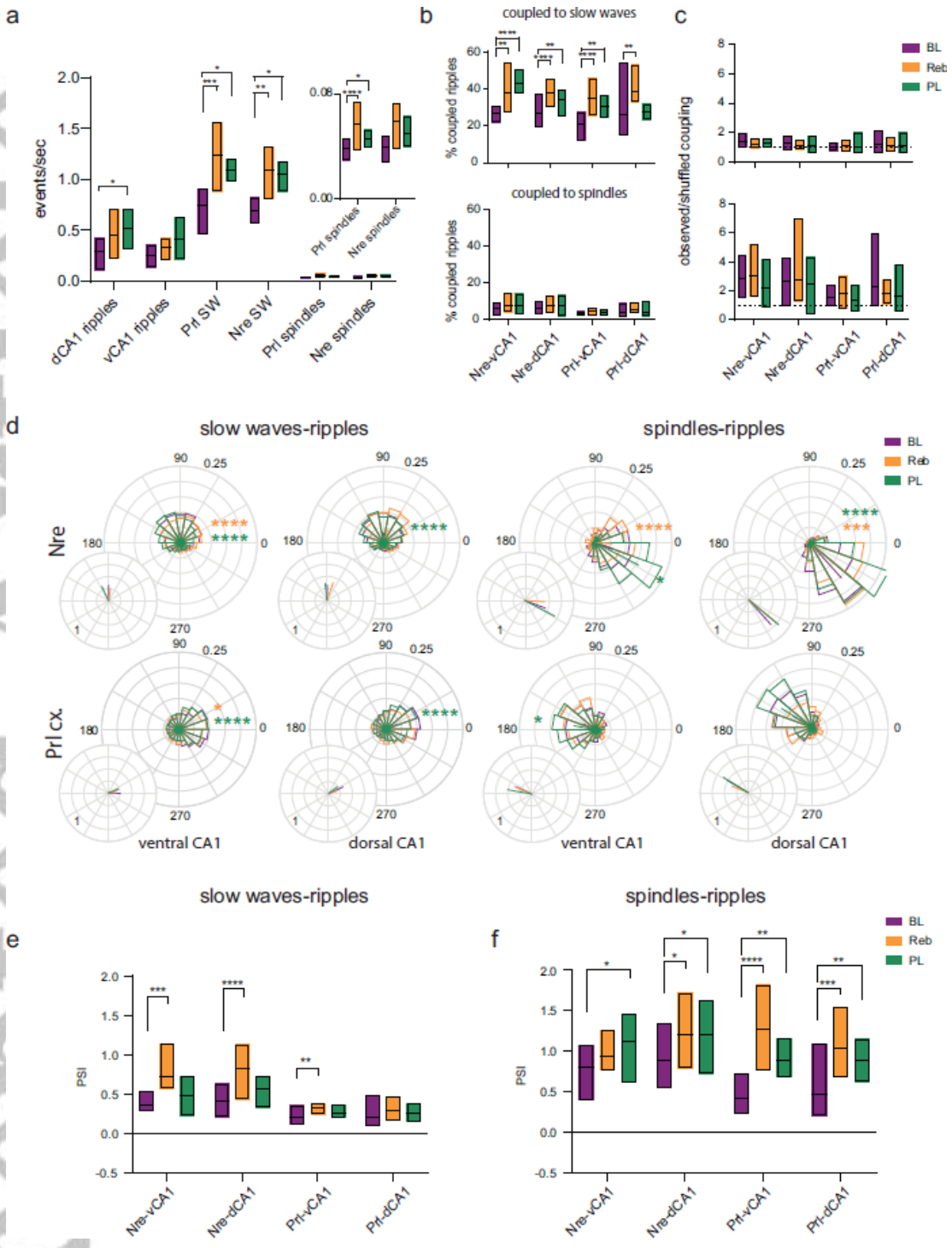


**Figure 2: Coupling of cortical and thalamic slow waves and spindles and hippocampal ripples.**

a) Box plots from minimal to maximal value with indicated mean showing the average densities of slow waves, spindles, and ripples during baseline sleep (BL), rebound sleep (Reb) and post-learning sleep (PL). Inset shows zoomed in values of spindle densities. *P<0.05, **P<0.01, ***P<0.001, ****P<0.0001 using one-way ANOVA followed by Dunnett's test for multiple comparisons.

b) Box plots from minimal to maximal value with indicated mean showing the average percentage of co-occurrence of ripples coupled with slow waves (top) or spindles (bottom) for

all detected ripples. *P<0.05, **P<0.01, ***P<0.001, ****P<0.0001 using One-way ANOVA followed by Dunnett's test for multiple comparisons.

c) Box plots from minimal to maximal value with indicated mean showing the average ratios of co-occurrence of ripples coupled with slow waves (top) or spindles (bottom) between observed data sets and shuffled data sets. No significant differences were measured using one-way ANOVA followed by Dunnett's multiple comparisons.

d) Normalized circular histograms showing the phase-amplitude coupling of hippocampal ripples to slow waves and spindles during baseline sleep (BL), rebound sleep (Reb) and post-learning sleep (PL). Thick lines represent mean circular vectors. The phase in the plots follows the cosine, so 0° marks the positive peak (UP state) and 180° marks the peak of the negative slope (DOWN state). Insets show a magnification of mean circular vectors with unit circle. All vectors were tested for non-uniformity with the Rayleigh test for non-uniformity. *P<0.05, **P<0.01, ***P<0.001, ****P<0.0001 using Parametric Watson-Williams multi-sample test for equal means as a one-way ANOVA test. If the assumptions of the test were not met, a non-parametric multi-sample test for equal medians was employed with Bonferroni correction of P-values.

e, f) Box plots from minimal to maximal value with indicated mean showing the average phase slope index (PSI). between ripples and slow waves (e) and ripples and spindles (f). *P<0.05, **P<0.01, ***P<0.001, ****P<0.0001 using One-way ANOVA followed by Dunnett's test for multiple comparisons.

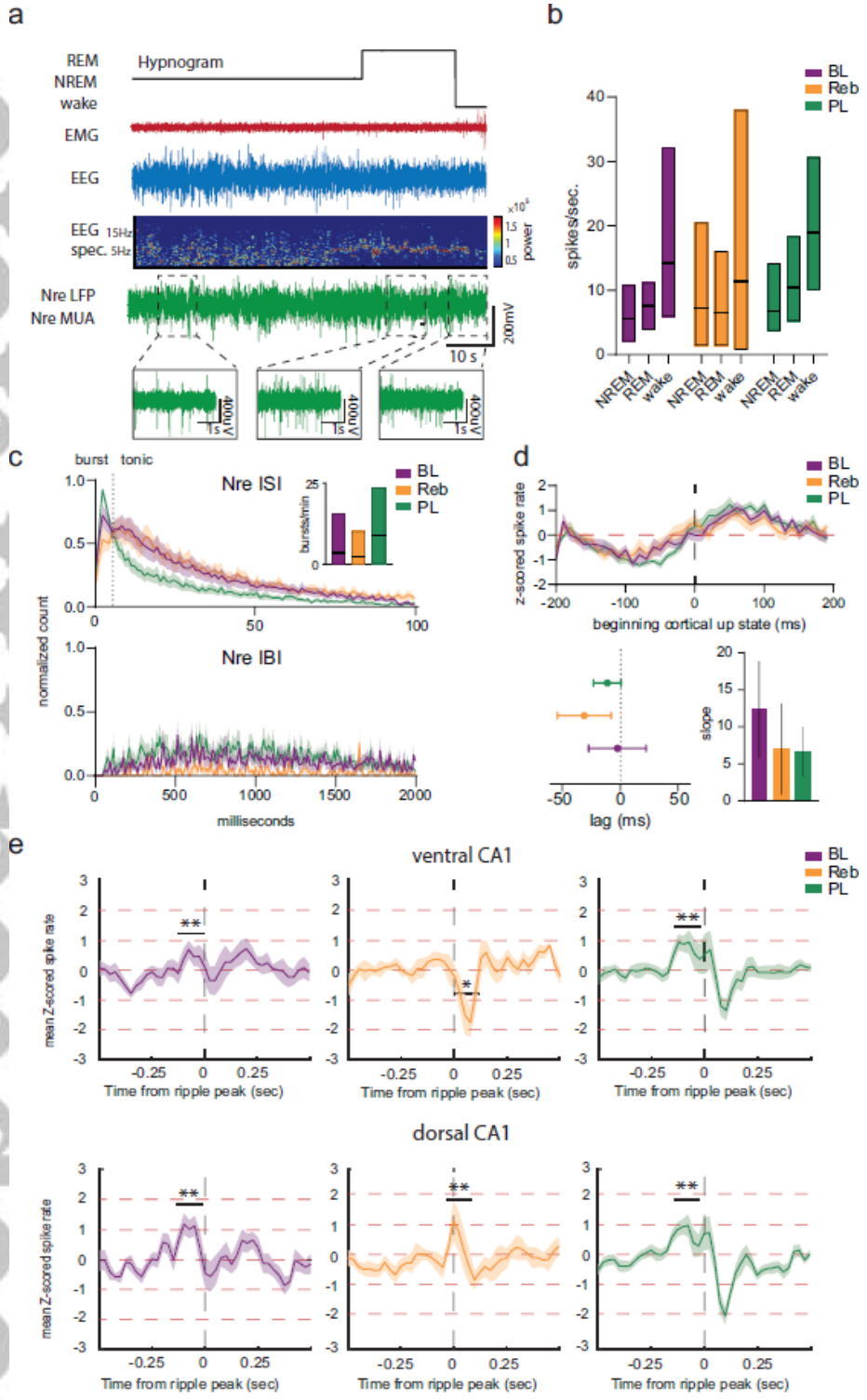


**Figure 3: Nre spiking behaviour during different vigilance states and in relation to cross-regional neuro-oscillations during baseline sleep (BL), rebound sleep (Reb) and post-learning sleep (PL).**

a) Representative hypnogram, EMG and EEG recordings, power spectrogram of the cortical EEG and multi-unit recordings from Nre across sleep-wake cycle. Insets: highpass filtering

showing NRE neuron spiking activity during wakefulness, NREM and REM sleep. Totally recorded units: n=11 cells from 8 animals in baseline sleep, n= 11 cells from 6 animals in rebound sleep, n= 10 cells from 6 animals in post-learning sleep.

b) Box plots from minimal to maximal value with indicated mean showing the average showing Nre spike rates across vigilance states during baseline sleep (BL), rebound sleep (Reb) and post-learning sleep (PL). No significant differences were measured using Two-way ANOVA with Dunnett's multiple comparisons test.

c) Distribution of inter-spike (top) and inter-burst intervals (bottom) in NREM sleep during baseline sleep (BL), rebound sleep (Reb) and post-learning sleep (PL). Nre cells show bursting behavior during NREM sleep. Inset, Box plots from minimal to maximal value with indicated mean showing the average of Nre cells bursts per minute during baseline sleep (BL), rebound sleep (Reb) and post-learning sleep (PL). No significant difference using One-way ANOVA with Dunnett's multiple comparisons.

d) Average spike rate +/- S.E.M. (z-score) of Nre neurons during a cortical UP state start (top). Time-lag +/- S.E.M. of Nre spike rate in relation to cortical UP state (bottom left) and Average slope +/- S.E.M. of Nre spike rate (bottom right) are shown. No significant difference One-way ANOVA followed by Dunnett’s test for multiple comparisons.

e) Average spike rates +/- S.E.M. (z-score) of Nre neurons during vCA1 (top) and dCA1 (bottom) ripples during baseline sleep (BL), rebound sleep (Reb) and post-learning sleep (PL). During rebound sleep, a decrease after the ripples was observed for vCA1 ripples, indicative of the end of the UP state. For dCA1 ripples, the peak was co-occurring with the ripples. Significance was tested by comparing peaks, or troughs, to baseline level firing at the beginning of the time window using a paired sign-rank test (see methods). *P<0.05, **P<0.01.

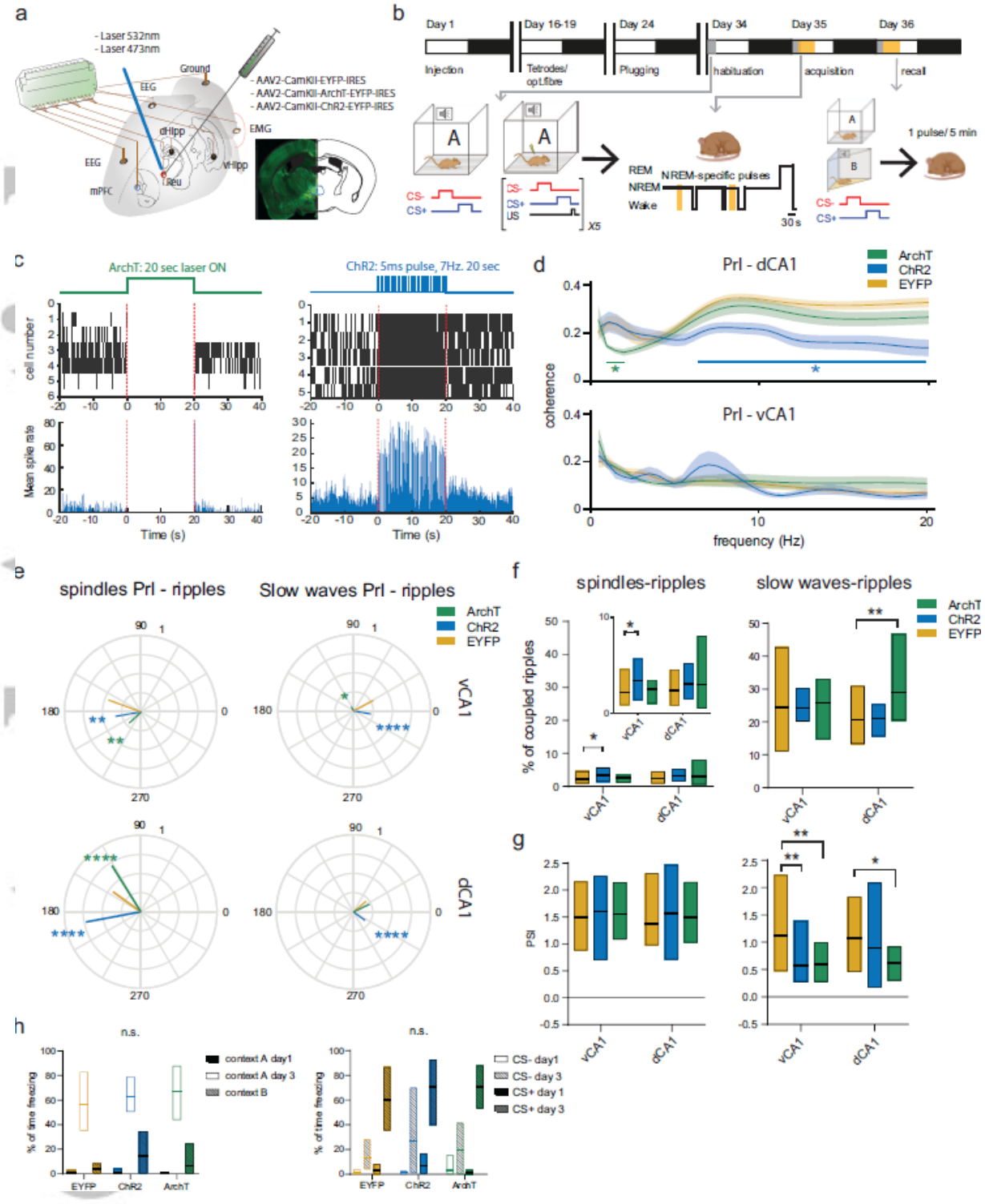


**Figure 4: Optogenetic manipulation of nucleus reuniens modulates cortico-hippocampal cross-frequency coupling.**

a) Schematic of the experimental setup showing viral transfection of Nre neurons, placement of tetrodes in Prl, Nre, vCA1 and dCA1, EEG/EMG electrodes, and optic fibre. Inset, Representative illustration of AAV2-CamKII-E1fa-ChR2-EYFP transfection in Nre.

b) Experimental timeline showing the time points of injection, implantation, habituation, fear conditioning and optogenetic activation or silencing. Activation protocol consisted of 140 laser pulses à 5ms seconds duration at 7Hz for 20 seconds. Silencing protocol consisted of turning the laser ON for 20 seconds.

c) Representative rasterplot (top) and average spike rates (bottom) of Archt (left)- and ChR2 (right)-expressing Nre neurons during optogenetic silencing (20s continuous illumination) and activation (5-ms pulses at 7Hz over 20 seconds), respectively.

d) Average coherence +/- S.E.M. between Prl and dCA1 (top) or vCA1 (bottom) during optogenetic activation (blue) or silencing (green) and control mice (yellow, N = 6 mice in each group). *P<0.05, using Two-way ANOVA with Dunnett's multiple comparisons.

e) Circular histogram showing the normalized phase-amplitude coupling of hippocampal vCA1 (top) and dCA1 (bottom) ripples to spindles (left) and slow waves (right) in Archt (green), ChR2 (blue) and control mice (yellow, N = 6 mice in each group). Colored lines represent mean circular vectors. *P<0.05, **P<0.01, ***P<0.001, ****P<0.0001 using Parametric Watson-Williams multi-sample test for equal means as a one-way ANOVA test. If the assumptions of the test were not met, a non-parametric multi-sample test for equal medians was employed with Bonferroni correction of P-values.

f) Box plots from minimal to maximal value with indicated mean showing the average percentage of co-occurrence of vCA1 and dCA1 ripples with spindles (left, inset shows magnification) or slow waves (right) during optogenetic stimulation, silencing, and control conditions. *P<0.05, **P<0.01, using One-way ANOVA with Dunnett's multiple comparisons.

g) Box plots from minimal to maximal value with indicated mean showing the phase slope index (PSI) between vCA1 and dCA1 ripples and cortical spindles (left) or slow waves (right). *P<0.05, **P<0.01, using One-way ANOVA with Dunnett's multiple comparisons.

h) Box plots from minimal to maximal value with indicated mean showing the average percentage of freezing behavior of ArchT (green), ChR2 (blue) and control (yellow) mice (N = 6 per group) during re-exposure to previous contextual (left), or discrimination (right) cues after acquisition of an auditory contextual fear conditioning test and optogenetic manipulation of Nre neuron activity (see panel b for timeline). No significant differences between the conditions were observed using two-way ANOVA followed by Dunnett's multiple comparisons test.

The study demonstrates that nucleus reuniens of the thalamus is electrophysiologically connected and that it regulates cortico-hippocampal coupling of slow waves, spindles, and ripples.